NAVAL POSTGRADUATE SCHOOL

MONTEREY, CALIFORNIA

THESIS

THE INFLUENCE OF PROTECTIVE POUCHES ON THE DEVELOPMENT AND INTENSIFICATION OF HURRICANE ETA (2020)

by

Nicohl M. Corretjer

June 2023

Thesis Advisor: Michael T. Montgomery
Co-Advisor: Mark A. Boothe

THIS PAGE INTENTIONALLY LEFT BLANK

REPORT DOCUMENTATION PAGE	*Form Approved OMB No. 0704-0188*

Public reporting burden for this collection of information is estimated to average 1 hour per response, including the time for reviewing instruction, searching existing data sources, gathering and maintaining the data needed, and completing and reviewing the collection of information. Send comments regarding this burden estimate or any other aspect of this collection of information, including suggestions for reducing this burden, to Washington headquarters Services, Directorate for Information Operations and Reports, 1215 Jefferson Davis Highway, Suite 1204, Arlington, VA 22202-4302, and to the Office of Management and Budget, Paperwork Reduction Project (0704-0188) Washington, DC, 20503.

1. AGENCY USE ONLY *(Leave blank)*	**2. REPORT DATE** June 2023	**3. REPORT TYPE AND DATES COVERED** Master's thesis

4. TITLE AND SUBTITLE
THE INFLUENCE OF PROTECTIVE POUCHES ON THE DEVELOPMENT AND INTENSIFICATION OF HURRICANE ETA (2020)

5. FUNDING NUMBERS

6. AUTHOR(S) Nicohl M. Corretjer

7. PERFORMING ORGANIZATION NAME(S) AND ADDRESS(ES)
Naval Postgraduate School
Monterey, CA 93943-5000

8. PERFORMING ORGANIZATION REPORT NUMBER

9. SPONSORING / MONITORING AGENCY NAME(S) AND ADDRESS(ES)
N/A

10. SPONSORING / MONITORING AGENCY REPORT NUMBER

11. SUPPLEMENTARY NOTES The views expressed in this thesis are those of the author and do not reflect the official policy or position of the Department of Defense or the U.S. Government.

12a. DISTRIBUTION / AVAILABILITY STATEMENT
Approved for public release. Distribution is unlimited.

12b. DISTRIBUTION CODE
A

13. ABSTRACT (maximum 200 words)

This thesis investigates the development of Hurricane Eta (2020) and its rapid intensification in the Western Caribbean during the late hurricane season. This study aims to show that the different stages of development of the system are supported by the marsupial paradigm. This paradigm requires, for tropical cyclogenesis, the existence of a protective pouch defined by a dividing streamline with a recirculating flow in a comoving frame of reference, which in the Atlantic is often associated with a westward-tracking African easterly wave. Global Model Analyses were examined in a comoving frame and indeed the precursor to Hurricane Eta was determined to have originated over Africa and then tracked westward over the Atlantic. Moreover, thorough examination of the model analyses allowed for a careful study of the interaction of multiple vortices within the pouch. Specifically, as the pouch crossed the central Atlantic, the separation distance between the two vortices within the pouch increased and then subsequently decreased as they merged and came into vertical alignment soon before formation as a tropical depression. The rapid intensification phase of Hurricane Eta immediately before landfall in Nicaragua is described also by examining moisture, relative vorticity, and vertical wind shear.

14. SUBJECT TERMS
marsupial paradigm, tropical cyclone formation, tropical cyclone intensification, 2020 Atlantic hurricane Season, Caribbean Sea, Okubo-Weiss parameter, pouch, hurricane Eta

15. NUMBER OF PAGES
79

16. PRICE CODE

17. SECURITY CLASSIFICATION OF REPORT	**18. SECURITY CLASSIFICATION OF THIS PAGE**	**19. SECURITY CLASSIFICATION OF ABSTRACT**	**20. LIMITATION OF ABSTRACT**
Unclassified	Unclassified	Unclassified	UU

NSN 7540-01-280-5500

Standard Form 298 (Rev. 2-89)
Prescribed by ANSI Std. 239-18

THIS PAGE INTENTIONALLY LEFT BLANK

Approved for public release. Distribution is unlimited.

THE INFLUENCE OF PROTECTIVE POUCHES ON THE DEVELOPMENT AND INTENSIFICATION OF HURRICANE ETA (2020)

Nicohl M. Corretjer
First Lieutenant, United States Air Force
BS, University of Missouri, Columbia, 2020

Submitted in partial fulfillment of the
requirements for the degree of

MASTER OF SCIENCE IN METEOROLOGY

from the

NAVAL POSTGRADUATE SCHOOL
June 2023

Approved by: Michael T. Montgomery
Advisor

Mark A. Boothe
Co-Advisor

Wendell A. Nuss
Chair, Department of Meteorology

THIS PAGE INTENTIONALLY LEFT BLANK

ABSTRACT

This thesis investigates the development of Hurricane Eta (2020) and its rapid intensification in the Western Caribbean during the late hurricane season. This study aims to show that the different stages of development of the system are supported by the marsupial paradigm. This paradigm requires, for tropical cyclogenesis, the existence of a protective pouch defined by a dividing streamline with a recirculating flow in a comoving frame of reference, which in the Atlantic is often associated with a westward-tracking African easterly wave. Global Model Analyses were examined in a comoving frame and indeed the precursor to Hurricane Eta was determined to have originated over Africa and then tracked westward over the Atlantic. Moreover, thorough examination of the model analyses allowed for a careful study of the interaction of multiple vortices within the pouch. Specifically, as the pouch crossed the central Atlantic, the separation distance between the two vortices within the pouch increased and then subsequently decreased as they merged and came into vertical alignment soon before formation as a tropical depression. The rapid intensification phase of Hurricane Eta immediately before landfall in Nicaragua is described also by examining moisture, relative vorticity, and vertical wind shear.

THIS PAGE INTENTIONALLY LEFT BLANK

TABLE OF CONTENTS

THIS PAGE INTENTIONALLY LEFT BLANK

LIST OF FIGURES

LIST OF ACRONYMS AND ABBREVIATIONS

AEJ	African Easterly Jet
AEW	African Easterly Wave
CL	Critical Latitude
GOES	Geostationary Operational Environmental Satellite
IR	Infrared
MP	Marsupial Paradigm
NHC	National Hurricane Center
NOAA	National Oceanic and Atmospheric Administration
OW	Okubo-Weiss
PV	Potential Vorticity
RH	Relative Humidity
RI	Rapid Intensification
SAL	Saharan Air Layer
SST	Sea Surface Temperature
TC	Tropical Cyclone
TD	Tropical Depression
TS	Tropical Storm
TPW	Total Precipitable Water
UTC	Coordinated Universal Time
ZULU	Time zone indicator for Universal Time

THIS PAGE INTENTIONALLY LEFT BLANK

ACKNOWLEDGMENTS

My deepest gratitude to my advisory team, Dr. Michael T. Montgomery, and Mr. Mark Boothe. Thank you for your continued advice and help during the entire process of this thesis.

I am very grateful to my family, my mom Marilia Acevedo Torres, my dad Peter Corretjer, and my sister Marieliette Corretjer, for always supporting me in my endeavors to further my education and my knowledge in the scientific fields. I would also like to thank my friends, Lt Mamott and Lt Huff. Lastly, I would like to thank Coco and Benito for their constant support.

THIS PAGE INTENTIONALLY LEFT BLANK

I. INTRODUCTION

A. THEORY

Tropical cyclones (TCs) have been one of the most destructive forces of nature worldwide since before humans walked the earth. Between 1980 and 2021, hurricanes cost the United States over $1.1 trillion in damages and took 6,697 lives, far more costly than other weather disasters. Our national statistics show how big of a concern these weather phenomena are, yet the global impact of storms of this magnitude is even more concerning. The recurrence of storms in certain regions also has an enormous negative impact on the socioeconomic condition of the affected countries. This is a call to action not only for our own national scientists, but understanding these cyclones requires collaboration on a global scale. Our technological and scientific advances have helped meteorologists track these phenomena earlier and with greater certainty than ever before in history (NOAA, 2022).

One prominent theory concerning the genesis of these storms was developed in 1975 (Gray 1975). It introduced six major physical parameters in the ocean and atmosphere required for hurricane genesis. The sea surface temperature (SST) and the top 200 feet of the ocean below must be greater than 79°F. The deflective force known as the Coriolis force, which is proportional to the product of the local vertical rotation of the Earth and the horizontal velocity of an air parcel, generates the cyclone's swirling circulation in the lower atmosphere by deflecting air motion that is drawn inwards by thunderstorm activity at interior radii. The implication of this deflective process is that TCs typically do not form close to the equator where the Coriolis effect vanishes. However, tropical storms are not observed to form spontaneously. Even with a nonzero Coriolis effect, some local low-level rotation is found to be necessary to establish the concentrated rotation of tropical storms. The larger the net rotation, the higher the likelihood of genesis. High mid-tropospheric humidity supports persistent deep convection, which in turn supports low-level convergence of moist air. Because of the link between the low-level inflow and the tangential circulation noted above, sustained low-level convergence is a vital ingredient of TC genesis. Finally, low vertical wind shear of horizontal winds between the lower and

upper atmosphere allows for persistent deep cumulonimbus convection and vertical coupling between the lower and upper tropospheric flows (Gray 1977).

Although we continue to use Gray's parameters as part of our modeling software and analysis, we still observe deficiencies in the forecasts. For example, many disturbances crossing tropical regions typically satisfy these conditions yet still fail to become tropical depressions. Scientists have been trying to fill the gaps and find evidence of additional key phenomena to improve predictions and decrease the devastating results of late preparation for tropical cyclones.

A new conceptual model for TC formation, referred herein to as the marsupial paradigm (MP), was established in 2009 by Dunkerton, Montgomery, and Wang (Dunkerton et al. 2009). The new model used global forecasting models to predict the preferred location for hurricane genesis. Analysis from the past several years has allowed a probability of formation to be developed also. This system often predicts the formation of TCs days earlier than operational forecasting techniques by identifying a protective pouch using a comoving reference frame, a semi-Lagrangian framework, instead of the commonly used Earth-relative framework. The model is intrinsically capable of analyzing the development of systems via three different pathways depending on the global region. Since the storm under investigation in this thesis formed in the Atlantic basin, we will provide a brief review of the paradigm from an Atlantic-basin perspective, following Dunkerton et al. 2009.

The overarching tenet of the marsupial paradigm is that tropical cyclogenesis requires the formation of a quasi-closed recirculating region around a disturbance associated with an African Easterly Wave (AEW), or easterly wave originating from disturbances within the Inter-Tropical Convergence Zone (ITZC). The parameters for optimal TC genesis and intensification are found within this area, the so called "pouch." The pouch acts to protect the proto-vortex within the pouch circulation from external degrading factors like wind shear and intruding dry air, like the Saharan Air Layer (SAL) in the Atlantic basin, and also fosters moisture containment. The pouch is tracked using a comoving reference frame as previously mentioned. In this way we can identify a region within the wave's trough that resembles a "cat's eye," a small, but finite amplitude vortical

circulation that is effectively isolated from the environment and subject to advection in opposite directions of the locally vortical flow (Dunkerton et al. 2009). The now visible vortex flow and the line formed from the wave's trough forms what we call the Kelvin cat's eye as illustrated in Figure 1. For a developing tropical cyclone in association with a tropical wave, the pouch moves along with its wave across the Atlantic and later the Caribbean depending on its trajectory. If the conditions remain favorable within the pouch the Okubo-Weiss (OW) and vorticity progressively increase as the wave disturbance becomes a depression and sometimes a hurricane (Dunkerton et al. 2009).

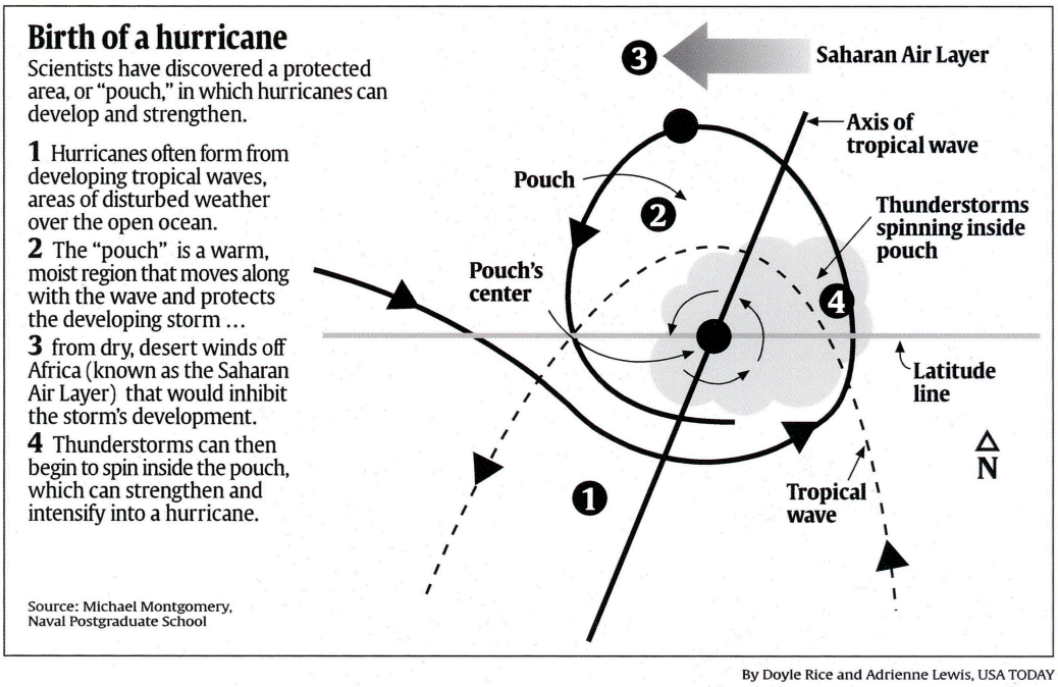

Figure 1. Marsupial Paradigm. Source: Rice (2008).

Two key parameters are used in this work to find the presence of these pouches: the relative vertical vorticity (ζ) and the Okubo Weiss parameter (OW). The relative vertical vorticity, as defined by Equation (1), is a measure of the local rotation in a fluid flow and is calculated from the vertical component of the curl of the velocity vector (American Meteorological Society [AMS] 2014).

$$\zeta = \hat{\mathrm{k}} \cdot \nabla \times \vec{u} = \frac{\partial \mathrm{v}}{\partial \mathrm{x}} - \frac{\partial u}{\partial y} \tag{1}$$

The OW parameter, as defined by Equation (2), is an alternative method of measuring vortical flow. Positive OW identifies "the shape-preserving component of a vortical flow" while negative OW indicates a flow dominated by shear and strain (Dunkerton et al. 2009). In positive OW regions, the vorticity tends to remain persistent, while in the negative OW regions the vorticity tends to be irreversibly deformed and stretched into oblivion (Dunkerton et al. 2009).

$$OW = \varsigma^2 - S_1^2 - S_2^2 = (V_x - U_y)^2 - (U_x - V_y)^2 - (V_x + U_y)^2 \quad (2)$$

In the defining equation for OW, ζ denotes relative vertical vorticity, $S_1 = U_x - V_y$ denotes the horizontal strain deformation and $S_2 = V_x + U_y$ which denotes the horizontal shear deformation (Dunkerton et al. 2009).

In their paper, Dunkerton et al. articulated three new hypotheses (H1-H3) for the process of tropical cyclogenesis. The three hypotheses are linked to the formation of a cyclonic Kelvin cat's eye circulation or protective pouch. The first hypothesis is the following:

> H1. Proto-vortex cyclonic eddies instrumental in TC formation are intimately associated with the parent wave's critical latitude in the lower troposphere. The critical layer and Kelvin cat's eye within, formed as a result of the wave's finite-amplitude interaction with its own critical latitude, contain a region of cyclonic rotation and weak straining/shearing deformation in which synoptic waves and mesoscale vorticity anomalies, moving westward together, amplify and aggregate on a nearly zero relative mean flow. This multi-scale interaction provides a dynamical pathway to "bottom-up" development of the proto-vortex from below. (Dunkerton et al. 2009)

The first hypothesis describes a bottom-up TC development process, wherein vorticity anomalies within the trough of a parent wave in an area of low shear start developing a strong vortex from the bottom of the system to the top. The first hypothesis points also to the formation of a cat's eye circulation, which originates from the interaction of the wave with its critical latitude (CL).

The CL is defined as an area where "the intrinsic wave frequency goes to zero" (Dunkerton et al. 2009). For disturbances originating in the African easterly jet or Inter-Tropical Convergence Zone (ITCZ), the CL is located "south of the southernmost latitude where the effective beta is zero" (Dunkerton et al. 2009 page 5593). The CL has to occur in the lower troposphere in order to have the necessary upward convective heating that will moisten the vertical air column with minimal vertical wind shear (Dunkerton et al. 2009). The equation defining the CL is given as

$$c=k*U, \tag{3}$$

where U is the mean flow vector, k is the dimensionless unit vector in the direction of wave propagation, and c is the wave's phase speed (Dunkerton et al. 2009).

The second hypothesis is the following:

> H2. The critical-layer cat's eye of the parent wave provides a set of quasi-closed material contours inside of which air is repeatedly moistened by convection, protected to some degree from lateral intrusion of dry air and impinging vertical shear, and (thanks to its location near the critical latitude) able to keep pace with the parent wave until the proto-vortex has strengthened into a self-maintaining entity. (Dunkerton et al. 2009)

The second hypothesis states how the pouch, which moves along with the parent wave, protects the proto-vortex within from dry air and vertical wind shear so that convection can progressively moisten the column. In this way, the pouch can develop into a stronger TC precursor. This is a crucial aspect in the Atlantic basin since dry air from the Saharan desert often plays a decisive role in the moisture levels required for TC formation (Dunkerton et al. 2009).

The third and last hypothesis is the following:

> H3. The parent wave is maintained and possibly enhanced by diabatically amplified eddies within the wave (proto-vortices on the mesoscale), a process favored in regions of small intrinsic phase speed. (Dunkerton et al. 2009)

This hypothesis suggests that smaller-scale diabatic vortices within the pouch help maintain the larger-scale wave. Once a tropical depression forms within the pouch, the developed proto vortex leaves the main wave and develops on its own.

Although the pouch and its associated sweet spot do not guarantee the formation of a tropical cyclone, the existence of a sustained pouch circulation, in combination with the key environmental parameters introduced by Gray, provides weather analysts with a higher formation certainty. The identification of these favorable parameters can assist analysts in identifying these storms earlier than ever before (Dunkerton et al. 2009).

In summary, when adopting the marsupial paradigm, the analysis of TC precursor disturbances in the Atlantic Basin begins by tracking the Okubo-Weiss parameter. This parameter is used to identify and track precursor African Easterly Waves (AEW) associated with the African Easterly Jet (AEJ) that flow from the Western African coast into the Atlantic, usually in the 650–700 mb layer of the atmosphere. An AEW is characterized by a weak low-pressure system in the lower troposphere. The trough of the wave acts as a source of cyclonic relative vertical vorticity for the incipient disturbance. To create a Kelvin cat's eye circulation, the wave interacts with its own critical latitude, an area south of the jet maximum, where the mean flow equals the wave's phase speed as defined by Equation (3). Figure 2 provides a conceptual model for the canonical flow setup. The emergent Kelvin's cat eye flow surrounds an area of almost zero mean relative flow where the relative flow inside and outside of the cat's eye flows in opposite directions (Dunkerton et al. 2009).

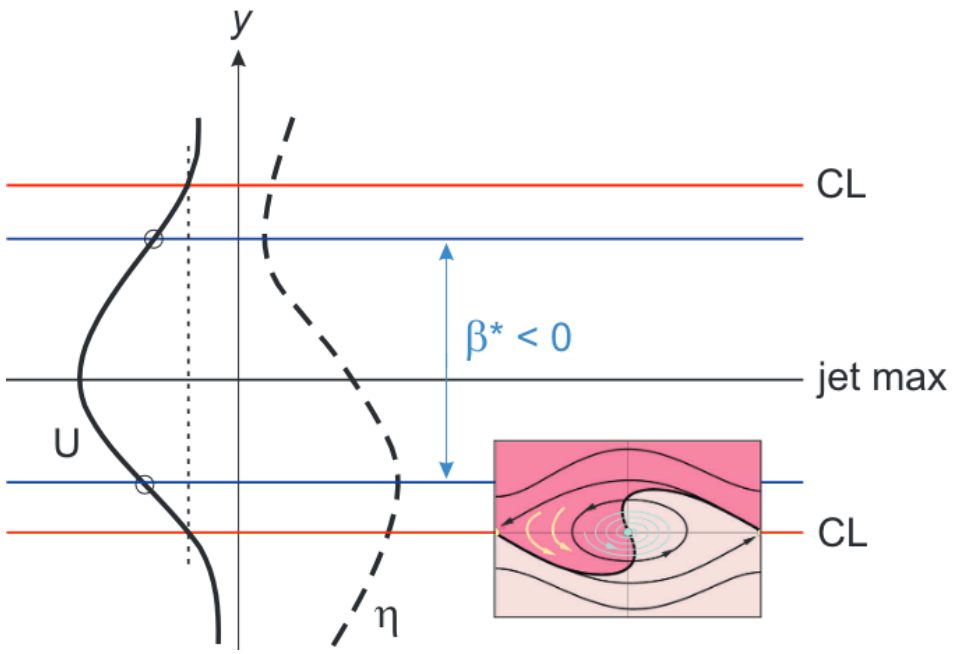

Critical latitude is where the wave's zonal phase speed coincides with the ambient mean flow.

Figure 2. Representation of the Cat's Eye Flow South of Jet Maximum. Source: Dunkerton et al. (2009).

B. CLIMATOLOGICAL ATLANTIC CONDITIONS

The 2020 hurricane season had some anomalies compared to a typical season, which yielded a more active late season. We will summarize some of the causes and effects of this hyperactivity. This context will help us understand the development and genesis of one of these storms.

The Atlantic hurricane season begins on June 1st and ends on November 30, usually having the peak number of storms and the highest intensity between late August and late September. There is typically a decrease in the number of storms and storm intensity in the late season. The late season is defined as ranging from October through November. (Klotzbach et al. 2022) After analyzing data from storms between 1991 to 2020, NOAA has calculated that on average there are 14 named storms, seven hurricanes, and three major hurricanes for the full season (Klotzbach et al. 2022). During the late season of the period from 1950–2019, the Atlantic basin had an average of 2.7 named storms, 1.5 hurricanes,

and 0.5 major hurricanes (Klotzbach et al. 2021). Between 1950 and 2019, only five major hurricanes formed during November, the last month of the Atlantic season (Klotzbach et al. 2021).

C. 2020 HURRICANE SEASON

During the 2020 hurricane season, scientists tracked 30 named storms, 14 of which became hurricanes, and seven of those became major hurricanes (Klotzbach et al. 2022). The season was not only highly active overall but had an abnormally active late season. The late season had seven named tropical storms, out of which six became hurricanes, five of which were major hurricanes. This is the highest number on record of major hurricanes in the late season of the Atlantic Basin; the old record was two major hurricanes. During the late season of 2020, five hurricanes formed in the Caribbean Sea, the highest amount ever recorded. Also, six out of the seven late season cyclones underwent rapid intensification (defined by NHC forecasters as an increase $\geq$ 30kt in 24hrs or less). This number of rapidly intensifying storms is another anomaly for the season and even rarer for the late season (Klotzbach et al. 2022).

These late-season anomalies have been linked to several environmental parameters, including vertical wind shear, sea surface temperature (SST), and atmospheric moisture analyzed through relative humidity (RH). Vertical wind shear is defined as "the change in the wind's direction and speed with height. This is a critical factor in determining whether severe thunderstorms will develop" (NOAA Weather Glossary 2022). A moderate intensity La Niña event was detected in 2020, and these events usually cause high-pressure systems in the western Atlantic leading to easterly winds in the Caribbean caused by these pressure systems. These easterlies, in addition to the easterly trade winds, are believed to decrease vertical wind shear in the west Atlantic and Caribbean, influencing the formation of TCs. The La Niña event, with strong easterly winds and minimal westerly wind, is most likely what drove the lower-than-average wind shear in the late season of 2020.

In October, the lower-than-average wind shear in the western Caribbean and Gulf of Mexico coincided with higher-than-average SST and moisture in the Caribbean (Klotzbach et al. 2022). Figure 3 compares the 2020 late season to recorded measurements since 1950. Lower than-average vertical wind shear in the southern tropical Atlantic may have aided the development of systems coming off Africa in late October. In early November, conditions in the western Caribbean had some of the most favorable potential intensity, midlevel moisture, and shear in the last 40 years. Potential Intensity (PI) is defined as "the maximum steady intensity a storm can achieve based on its energy cycle, in which the heat input by evaporation from the ocean, multiplied by a thermodynamic efficiency, is balanced by mechanical dissipation in the storm's atmospheric boundary layer" (Emanuel 1999, pp. 665–666).

$$V^2 = \frac{C_k}{C_D}\frac{T_s - T_o}{T_o}(k_s - k_a) \tag{4}$$

Here, V describes the maximum azimuthally and temporally averaged gradient wind speed at the top of the boundary layer, C_K and C_D are dimensionless coefficients describing enthalpy and momentum transfer at the sea surface, respectively; T_s is the absolute temperature of the sea surface and T_o is the absolute temperature at the top of the storm, k_s is the saturation enthalpy at the ocean's surface and k_a is the enthalpy of the boundary layer air at the top of the surface layer (~10 m) (Emanuel 1999).

The totality of the foregoing factors are believed to have led to the rapid intensification of November storms in 2020, including Hurricane Eta (Klotzbach et al. 2021).

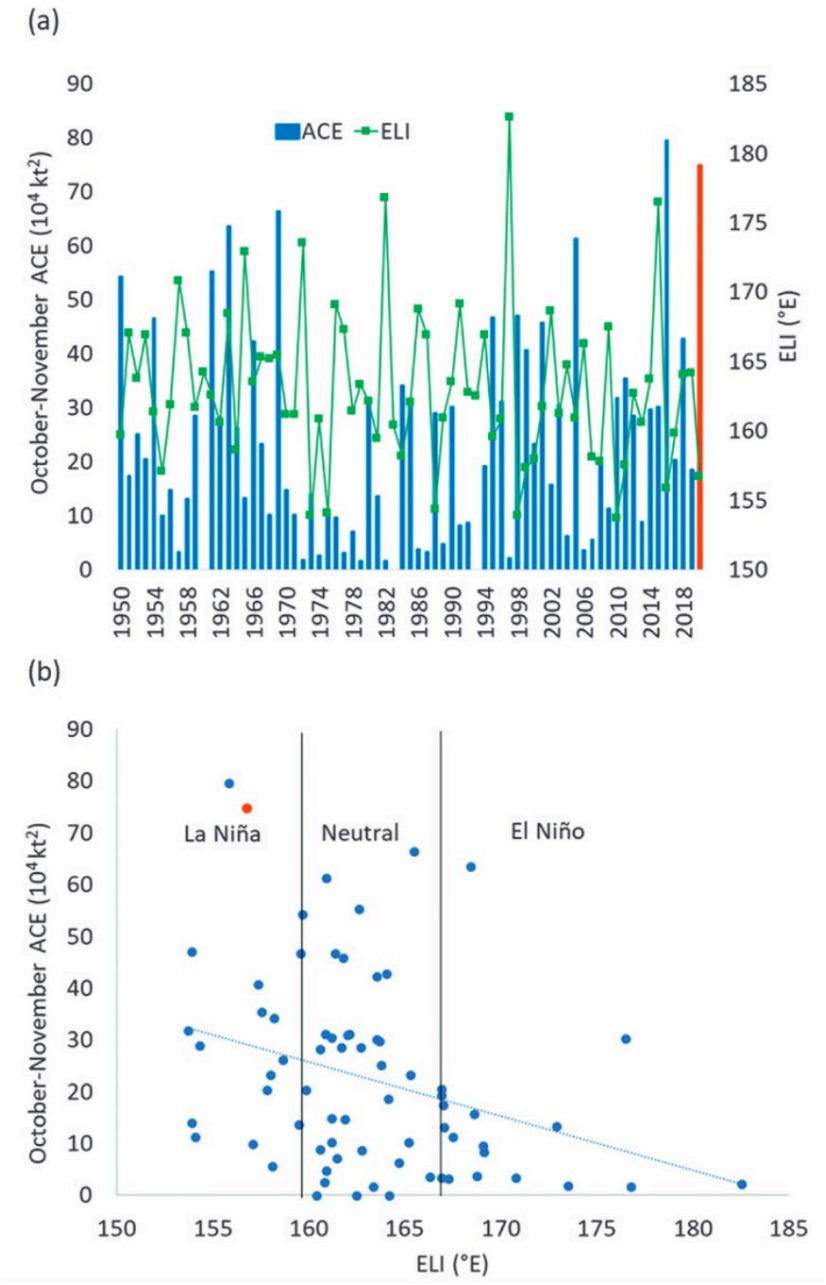

(a): The green line shows ELI, which is a measurement of average SST. "The ELI is calculated by averaging the longitude across the equatorial Pacific where the SST threshold for deep convection is met, a threshold defined as the SST averaged over the region from 5°S to 5°N." (Klotzbach et al. 2022) The blue bar shows yearly October-November accumulated cyclone energy (ACE) in the Atlantic, with 2020 highlighted in red. "Accumulated cyclone energy is an integrated metric accounting for frequency, intensity, and duration of storms and is calculated by squaring the maximum sustained wind speed at each 6-hourly interval when a tropical or subtropical cyclone has maximum sustained winds ≥ 34 kt (e.g., a named storm) and then dividing by 10,000." (Klotzbach et al. 2022) (b) Red dot is the ELI and Oct-Nov ACE for 2020. (Klotzbach et al. 2022)

Figure 3. Climatology vs. 2020 Season. Source: Klotzbach et al. (2022).

D. FOCUS OF THIS STUDY

Hurricane Eta (Figure 4) was the most catastrophic hurricane in the late 2020 season with the most fatalities and damages. Eta had four landfalls (Figure 5), the most for the season: one each in Nicaragua and Cuba, and two in Florida (Pasch et al. 2021). Eta had one of the strongest rapid intensifications for the season which caused damage across the Caribbean. Eta caused an estimated $1.5 billion in damages in the U.S. and an estimated $6.8 billion in total damages across different countries (Klotzbach et al. 2022). It was also responsible for 165 direct deaths in Central America and Mexico and seven direct deaths in the United States (Pasch et al. 2021).

The destruction that follows the path of hurricanes is also a large risk to national security. In the past, we have seen how these storms can destroy large military installations and supplies, affecting missions and putting our nation at risk during our most vulnerable. A prime example of this is Hurricane Michael (2018), a category 5 hurricane that made landfall in northern Florida in October of 2018. Initially, forecasters predicted the storm would make landfall as a category 2 hurricane and locals made preparations for such an event. Yet, the storm underwent rapid intensification and shifted northeastward after interacting with the southern edge of mid-latitude westerly winds causing it to have landfall near Tyndall Air Force Base (AFB) (Beven et al. 2019). Nobody was prepared for the magnitude of the storm that arrived. Hurricane Michael caused 16 direct deaths and about $25 billion in damages in the U.S., with over $3 billion in damages on Tyndall AFB alone (Beven et al. 2019). $618 million was sent for immediate repairs to the base after catastrophic destruction to the whole infrastructure (Reeves 2019). Rebuilding is still not complete, and this storm greatly affected the Air Force's mission in the area. Two years later, Hurricane Eta underwent a similar rapid intensification and now serves as a case study with which to examine and understand this dangerous process using the marsupial paradigm principles to ensure preparedness for these major natural disasters.

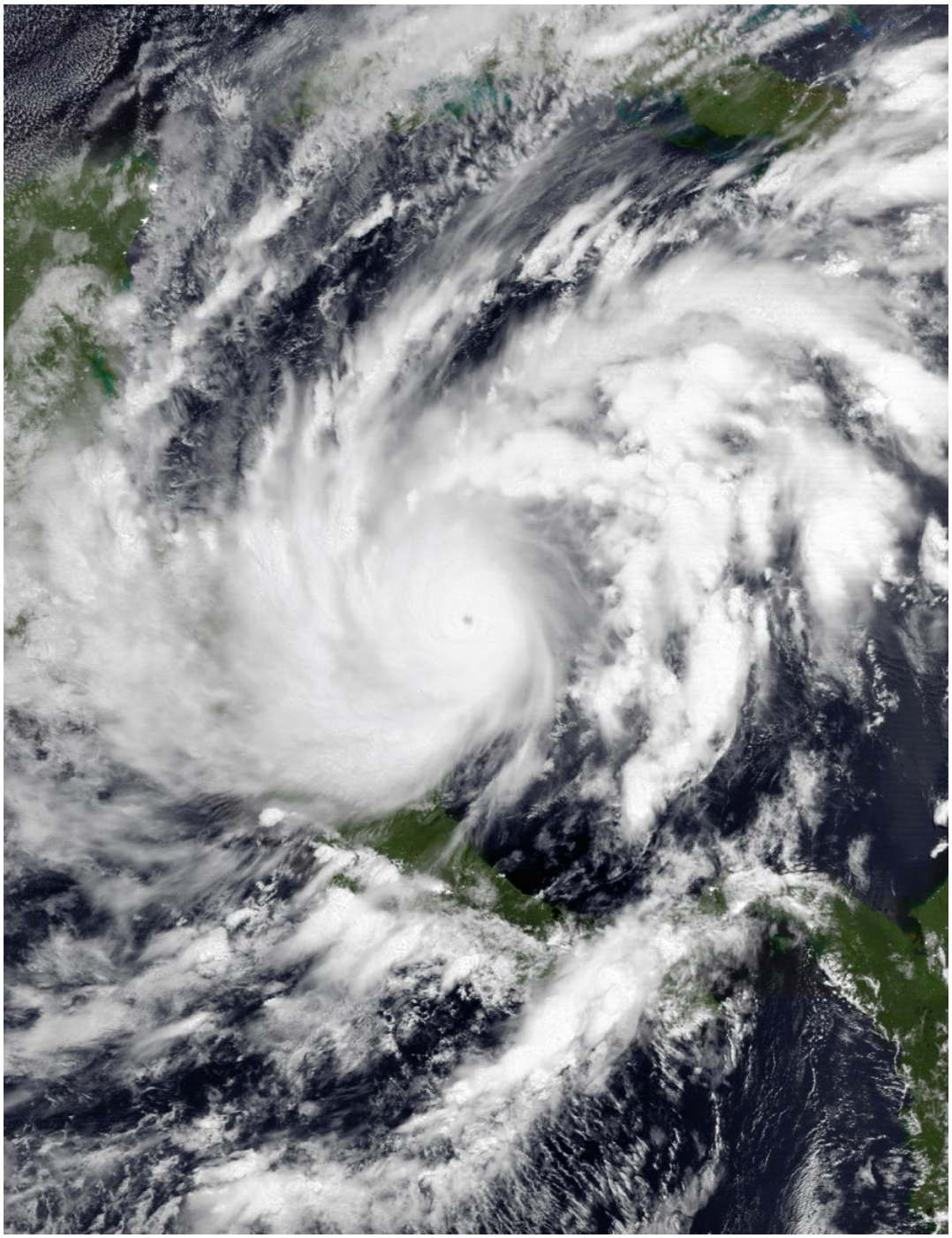

NASA's TERRA Moderate Resolution Imaging Spectroradiometer (MODIS) showing Hurricane Eta at 0640 UTC 3 November 2020.

Figure 4. Hurricane Eta Sat Image 3 Nov Source: NASA (2020).

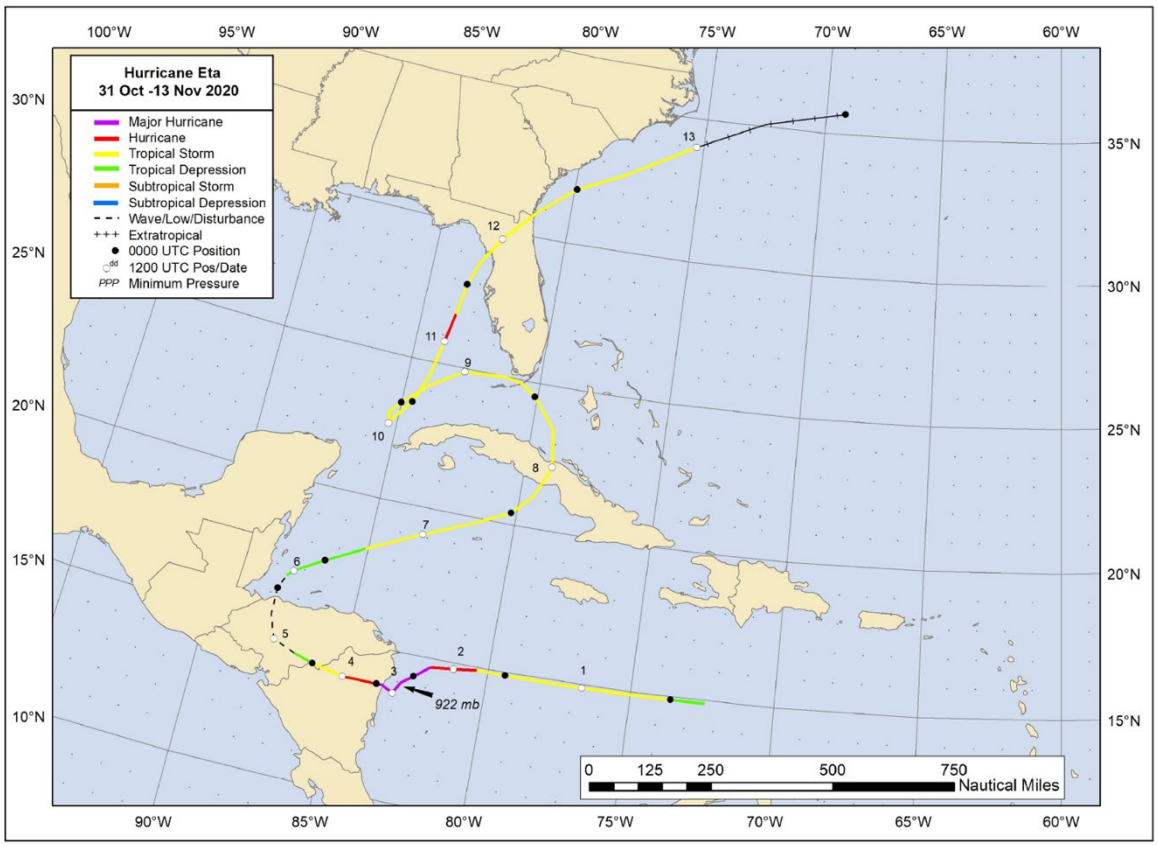

Figure 5. The Official Track of Hurricane Eta (2020).
Source: Pasch et al. (2021).

THIS PAGE INTENTIONALLY LEFT BLANK

II. METHODOLOGY

A. TECHNIQUE

Over five years ago, the concepts of the Marsupial Paradigm were utilized to develop a program that automatically identifies and tracks pouches in all tropical cyclone basins around the globe. The Monterey Research Group at the Naval Postgraduate School (NPS) has run the program using the operational 00 UTC GFS model run every day since April 2017. Diagnostic basin-scale and pouch-scale graphics of analyses and forecasts every 3 hours out to a 120-hour forecast are posted on a public website. Available products include pressure-level and time-height depictions of comoving streamlines, vorticity, and moisture, as well as a probability forecast of the likelihood of a developed tropical cyclone. During the 2020 season, the automatic tracking system first identified Eta's precursor at 00 UTC on 28 October 2020 on both the 700 and 850 mb levels, when the circulation was approaching South America near 8N, 48W. However, for this thesis, we did not use this automatic analysis; instead, through careful visual examination of GFS analyses, we were able to track the system almost a week earlier as the circulation emerged from Africa.

Our manual investigation of the precursor of Hurricane Eta followed the same process as Britton (2021) and McKaig (2021). We began to track the pre-TC system by using the NHC best track published in their Hurricane Eta report. The first published coordinate was at 18 UTC 31 October when the NHC declared the system a tropical depression. We then worked backward in time tracking a positive and coherent mesoscale OW feature in comoving fields in GFS analyses every six hours, at 00, 06, 12, and 18 UTC. We initiated our analysis using estimated zonal and meridional phase speeds extrapolated backwards from the NHC best track using the haversine equation to calculate distance on the oblate spherical surface of the Earth. We then displayed the GFS analysis of OW and phase speed dependent comoving streamlines using the Gridded Analysis and Display System (GrADS) developed by the center of Ocean-Land-Atmosphere Studies, Institute of Global Environment and Society at George Mason University. We examined the GFS

comoving analyses at both 700 and 850 mb to understand the structure of the circulation and to ascertain the level at which the circulation was stronger and presumably easier to track. After a position and pressure level was determined at a particular GFS analysis, the process was repeated for the prior six hourly synoptic time. This visual tracking process was an iterative process, that often required repeated assessments to ensure that we were tracking a persistent and coherent mesoscale OW feature with a representative set of phase speeds.

The comoving framework provides an enlightened depiction of a pouch that may develop into a TC. A key tool it provides is a depiction of westerlies on the southern side of a comoving circulation that the Earth-relative framework does not show until a tropical depression is already nearly formed. Figure 6 compares the two frameworks of the developed pouch at 06 UTC 23 October, which was $8\frac{1}{2}$ days before the first NHC advisory was issued for Tropical Depression 29L (eventually Hurricane Eta). While the Earth-relative framework depicts a trough associated with a large area of easterlies in an AEW (Figure 6, left), the comoving framework depicts a quasi-closed pouch with a cyclonic circulation that is moving westward at 7 m/s. The intersection of the wave's trough and critical latitude, which depicts the so-called "sweet spot," is collocated with an OW maximum (Figure 6, right). Note the similarity between the comoving example and the conceptual model of Figures 1 and 2.

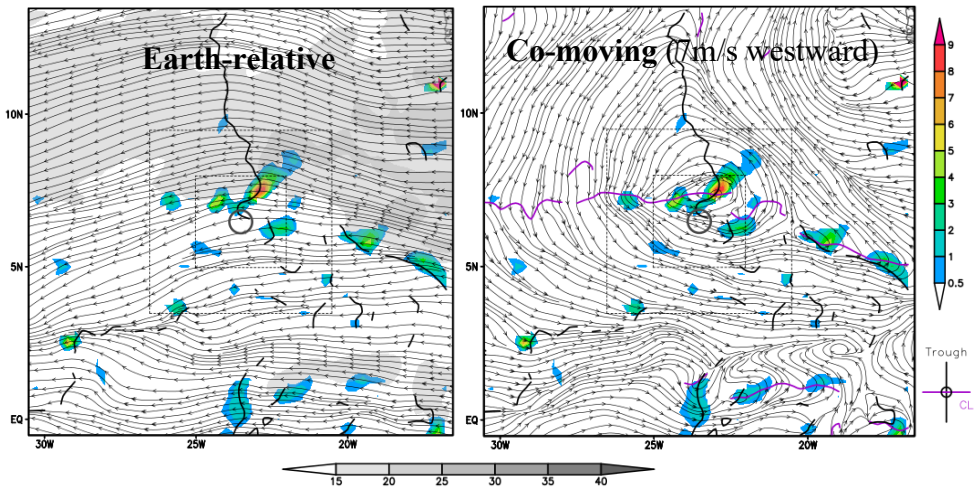

GFS analyses of 850 mb OW (color shading, units 10^{-9} s^{-2}) at 06 UTC 23 October 2020 overlaid with streamlines and wind speeds (grey shading, units kts) in the (left) Earth relative and (right) comoving framework. Thick black lines depict troughs; thick purple lines depict the comoving critical latitude. Central circle depicts location of comoving circulation center at the higher 700 mb level. Dashed boxes denote pouch-centered 3° x 3° and 6° x 6° boxes used in subsequent area-average calculations of important variable.

Figure 6. Earth-Relative vs. Pouch-Relative Framework

During our analysis of the track, we selected the intersection of the trough and critical latitude to the best of our abilities, however, there is room for error from the given GFS data. There were several times in the early phase of the precursor when the system weakened, and the GFS did not depict an intersection of a CL with the wave trough. At these times, we estimated the location of the center based on the wave's phase speed and our prior knowledge of where the system was confirmed later (with actual sweet spot data or NHC data). The analysis was an iterative process where estimates were used to find the appropriate location of the center of the pouch until the final and correct phase speeds were identified. Using the correct phase speeds, we could then detect the comoving flow/streamlines and properly locate the center of the flow/pouch. During the merger process of the system, it became difficult to trace the center of circulation, and multiple OW maxima were tracked instead. To track the system after development as Tropical Depression 29L, we simply used the coordinates published by the NHC to initiate the comoving plotting routine.

The initial level used for tracking the disturbance off the coast of Africa was the 700 mb level at 06 UTC 22 October 2020. This is the level where a coherent OW feature first emerged. This is also the approximate altitude from which the AEW associated with the AEJ usually emerges from in West Africa. After the wave emerged near the West African coast, we continued tracking and analyzing the wave and pouch at various levels in the atmosphere. We verified our original track with the vertical relative vorticity at the same intersection of the trough and critical latitude. We continued tracking the system at this level since it remained persistent for most of the genesis time. Whenever the system became more disorganized and multiple centers of OW emerged, we started tracking the different centers at the 850mb level, beginning at 18 UTC 25 October. Although the pre-Eta disturbance was tracked at a single pressure level, we typically analyzed data from three levels in the atmosphere, namely 700 mb, 850 mb, and 925 mb.

B. DATA

The data we gathered during our analysis yielded several results, including OW, relative vorticity, relative humidity, 200–850 mb "deep" shear, 500–850 mb "pouch" shear, winds, location of pouch center, equivalent potential temperature (θ_e), and vertical mass flux. Our model calculates the horizontal areal average of these variables in the GFS analyses, over 3° x 3° and 6° x 6° boxes centered on the pouch we selected. The data from these outputs were used to create time-height and time-series plots with MATLAB. The time-height plots include 19 different levels of the atmosphere from 100 mb to 1000 mb every 50 mb level. The time series plots use the same calculations but at the single pressure level at which the pouch is tracked. These diagnostic products provide a quantitative assessment of the state of the pouch flow during our system's development.

The pouch shear is a calculation of the difference of winds between the 500 mb and 850 mb levels at each grid point of the GFS output. We use this pouch shear to analyze whether low-level shear affects our system. The pouch shear is the most useful during the pre-genesis period because it focuses on the pressure levels that span the pouch. The deep shear is calculated using the difference in wind speeds between the 250 mb and 850 mb levels. The deep shear is a good way to estimate total wind shear across the tropical

troposphere and captures the wind shear associated with upper-level jets. For both types of vertical wind shear, the 3° x 3° and 6° x 6° boxes areal averages are averages of these vertical shear values at multiple GFS grid locations within the boxes, resulting in a single average vertical shear.

Equivalent potential temperature (θ_e) "is the potential temperature that a parcel of air would have if all its moisture were condensed and the resultant latent heat used to warm the parcel." The definition used in this thesis is given by Holton (2004 his equation 9.40, pg. 291): where θ denotes dry potential temperature, L_c is the latent heat of condensation, q is the water vapor mixing ratio of the initial state of the parcel. C_{pd} is the specific heat at constant pressure of dry air, and T_{LCL} is the temperature of the parcel if it expanded adiabatically until reaching saturation. It can be shown that θ_e is materially conserved for both dry and pseudo adiabatic displacements in the absence of heat and water vapor diffusion (Holton 2004).

$$\theta_e = \theta \exp\left(\frac{L_c q}{C_{pd} T_{LCL}}\right) \tag{5}$$

We used MATLAB to plot the track we constructed from our careful GFS analysis. This track was then compared with the total precipitable water (TPW) graphs from the University of Wisconsin that depict atmospheric moisture anomalies during the analysis time. The TPW product gives the total precipitable water in the vertical column per square meter. The TPW product provides an independent data source for assessing the track and motion of the tracked disturbance compared to our method based on the GFS analyses. This allows us to verify whether the high TPW values are on track with the location we propose for the pouches.

Imagery from NOAA's Geostationary Operational Environmental Satellite (GOES) system was gathered from their Comprehensive Large Array-Data Stewardship System. We specifically use infrared (IR) and visible satellite imagery from NOAA's GOES-16 to verify our model data outputs. This imagery is used to compare the location of our tracked pouch with the location, extent, and vigor of convection.

THIS PAGE INTENTIONALLY LEFT BLANK

III. ANALYSIS

One operational requirement for the National Hurricane Center (NHC) to initiate warnings on tropical systems is the presence of westerly winds on the south side of a circulation in an Earth-relative framework. This usually occurs immediately before the system intensifies into a tropical depression. In this chapter we track features in a superior semi-Lagrangian framework of the Marsupial Paradigm as summarized in the Introduction, a so-called "co-moving reference frame" that translates with the pre-TC disturbance. In this case, we are able to begin the analysis of the precursor of Hurricane Eta by tracking a persistent mesoscale feature with a high OW value as it moved westward off the coast of Africa. The co-moving framework generally reveals a disturbance with an approximately closed circulation at the level of maximum disturbance amplitude and with co-moving winds that are westerly on the south side of the circulation. This circulation can be detected one or more days prior to becoming a disturbance with a high likelihood of becoming a tropical depression according to hurricane forecasters.

The analysis presented below will examine both the formation and intensification phases of Eta (2020). For the formation phase, we present an in-depth dive into the small-scale weak circulations associated with the AEW that interacted with each other and ultimately merged to become Hurricane Eta at 06 UTC 2 November 2020. For the intensification phase, we present observational NHC data and our own personal analysis data associated with this small rapid intensification window. The time of analysis is summarized in Figure 7, which shows our analyzed track of Eta's main precursor disturbances and the TC that became Hurricane Eta.

During our in-depth analysis, we discovered two pouches (Figure 7, red and green tracks) that later merged via a quasi-direct cyclone interaction between 12 UTC 27 October and 06 UTC 30 October to form Hurricane Eta's precursor pouch. We also observed a time

of significant instability over the Atlantic, which started at 00 UTC on 23 October near 6.5° N, 20.8° W and ended at around 18 UTC 27 October near 9.87° N, 53.48° W. During this period, multiple convective vortices formed near or within the tracked pouch. The formation of these convective vortices and the ultimate merger just mentioned will be examined as part of our analysis of the formation of Eta.

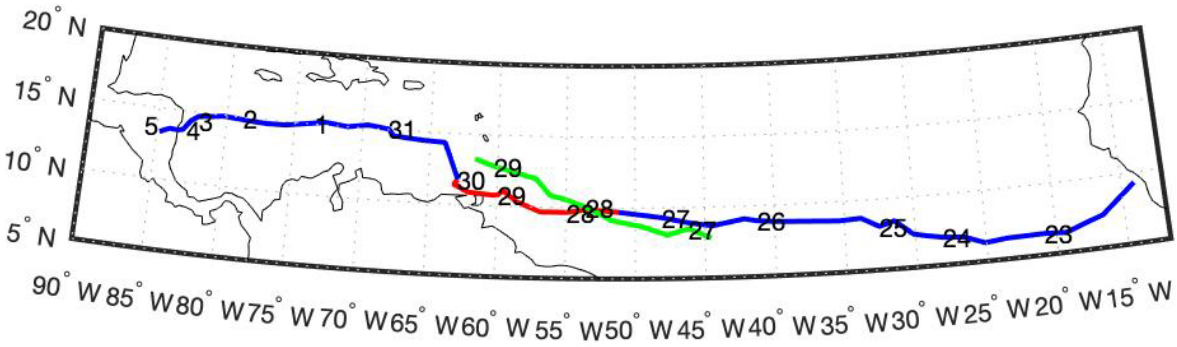

Track of precursor of and eventual Hurricane Eta from the African coast at 06 UTC 22 October until 12UTC 4 November 2020, soon after the first landfall in Nicaragua. Track based upon 6-hourly GFS analyses, with the date to the immediate right of the 00 UTC position for that date. Blue track indicates periods when a single feature is tracked. Red and green tracks indicate the period when two features that eventually merge were tracked.

Figure 7. Track of Precursor for Eta and Hurricane Eta in 2020

The NHC described that convection associated with Eta's precursor was weak and disorganized from the time it left African on 22 October 2020 until it strengthened on 29 October near the Windward Islands (Pasch et al. 2021). Total Precipitable Water (TPW) charts (University of Wisconsin) depict the westward movement of the zonally broad, moist AEW and pouch (Figure 8). The presence of multiple TPW maxima during the 25–29 October period highlight the disorganized nature of the pouch during the early period before consolidation into a single moist region occurred on 30 October.

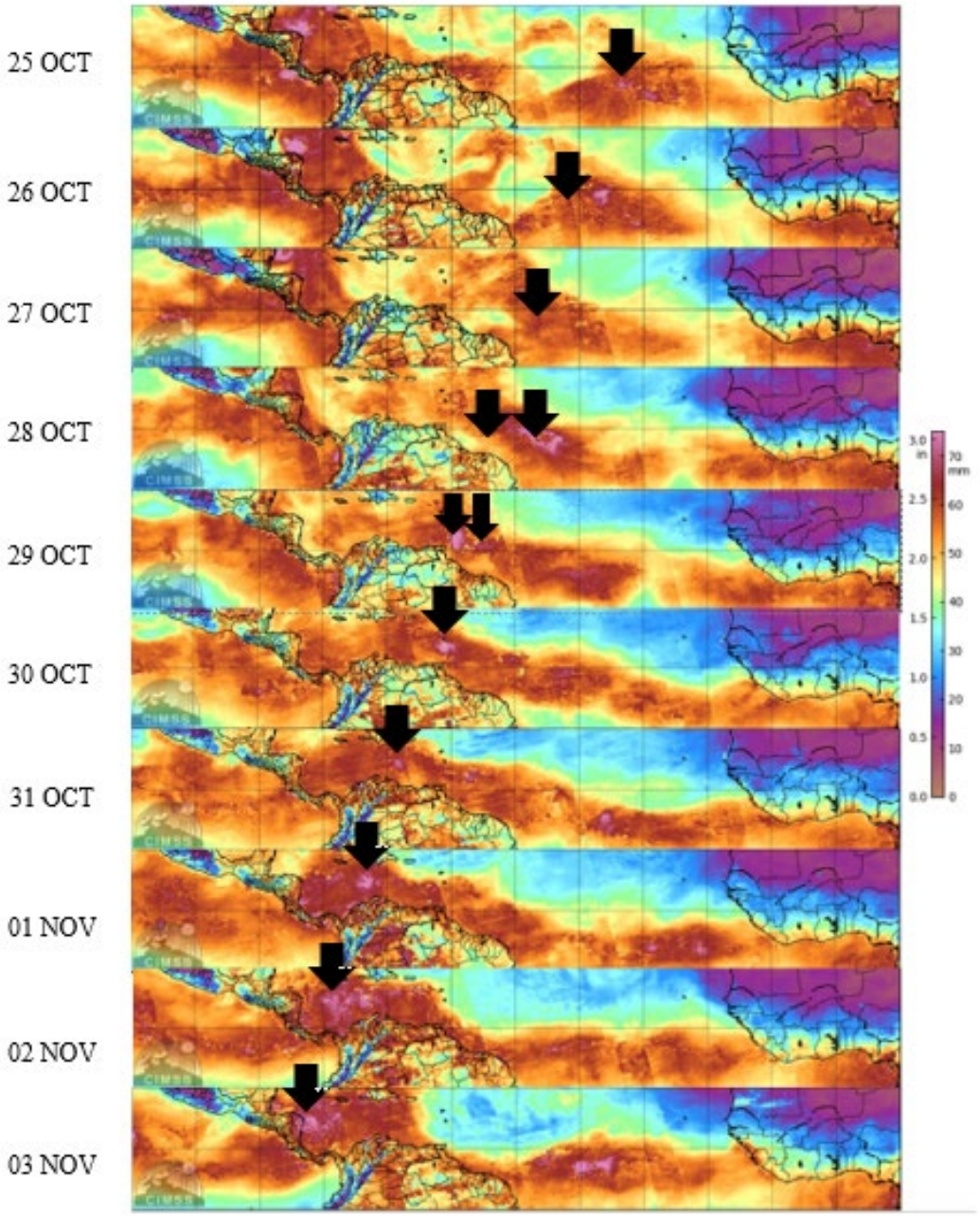

Total Precipitable Water (TPW) once a day at 00UTC from 23 October to 3 November 2020 (University of Wisconsin). Black arrows indicate the presence of a tracked feature.

Figure 8. Daily TPW at 00 UTC during 25 October to 3 November 2020

A. EARLY PHASE

Using our semi-Lagrangian manual analysis technique, we were able to identify a feature that later developed into Hurricane Eta as early as 06 UTC 22 October 2020 when an African Easterly Wave (AEW), moved off the coast of West Guinea (Figure 9, top left). Like most waves coming off Africa, the circulation was strongest near 700 mb; however, the 700 mb circulation was spatially tiny, with only a small area of positive OW (figure 9, top left). It was also confined to a thin layer, as evidenced by only northeasterly, non-circulating 850 mb winds with little to no OW and relative vorticity below the tracked 700mb feature (Figure 9, middle left). While the 850 mb wind field exhibits an area of cyclonic flow curvature with a modest area of positive OW (Figure 9, middle left) and a larger area of positive relative vorticity (Figure 9, bottom left), this curving area is near 7°N. This area was roughly 120n.mi. to the southwest of the tiny 700mb circulation. GOES infra-red (IR) satellite imagery indicates some convection at this time, especially to the south of the pouch center (Figure 10, bottom left). By 12 UTC 22 October, the 700 mb feature had tracked southwestward and was collocated with this area of low-level curvature (Figure 9, right). While the 850mb circulation is spatially larger and possesses higher values of OW and relative vorticity than the smaller 700mb circulation, the 850mb comoving streamlines depict an open circulation.

During this 6-hour period, as the circulation shifted southwestward, the disturbance moved away from a region of moderate vertical wind shear greater than 8 m s^{-1} (figure 10, top row). This is thought to have helped allow the circulation to persist. Meanwhile, the relative humidity (RH) at all levels increased drastically for two reasons. First, as depicted in (Figure 10, middle left), the area near 7°N was already moist with RH values greater than 85% at 06 UTC 22 October. The tracked feature then moved southwestward into that moist region (Figure 10, middle right). This region falls within the Inter-Tropical Convergence Zone (ITCZ) which was estimated to be centered between 6–7° N on that day (NOAA, 2020). Second, the AEW itself is moistened also. While the 700mb air with RH values exceeding 80% was limited to latitudes south of 8°N at 06 UTC (Figure 10, middle left), by 12 UTC, 80% RH values extended northward beyond 10°N (Figure 10, middle right). Interestingly, the location of the tracked 700mb circulation relative to convection as

seen in GOES infra-red (IR) imagery (Figure 10, bottom) indicates little change in convection over the six hours as the circulation remained near the northern edge of an area of unorganized convection.

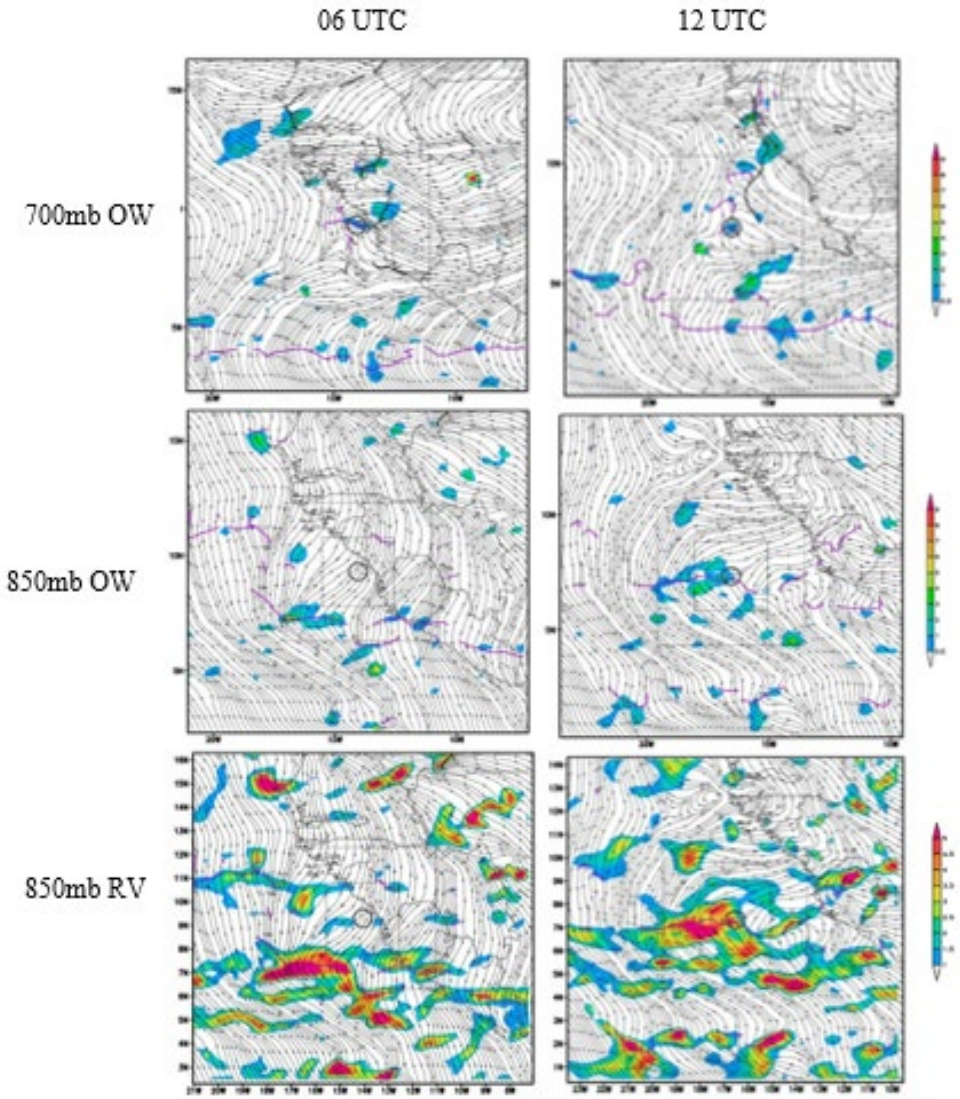

GFS analysis of OW (color shading) with wind speeds (grey shading) and comoving streamlines at 700mb (top row) and 850 mb (middle row) at 06 UTC (left) and 12 UTC (right) 22 October 2020. Bottom row depicts GFS analysis of 850 mb relative vorticity (shading) and comoving streamlines at the same times as above. Black circle in center indicates the location of the feature, which was tracked at 700mb at this time. Thick black lines indicate troughs, while thick purple lines indicate critical latitudes in the comoving flow (and these features appear in subsequent GFS analyses).

Figure 9. GFS Analysis of OW and Vorticity 22 October 2020

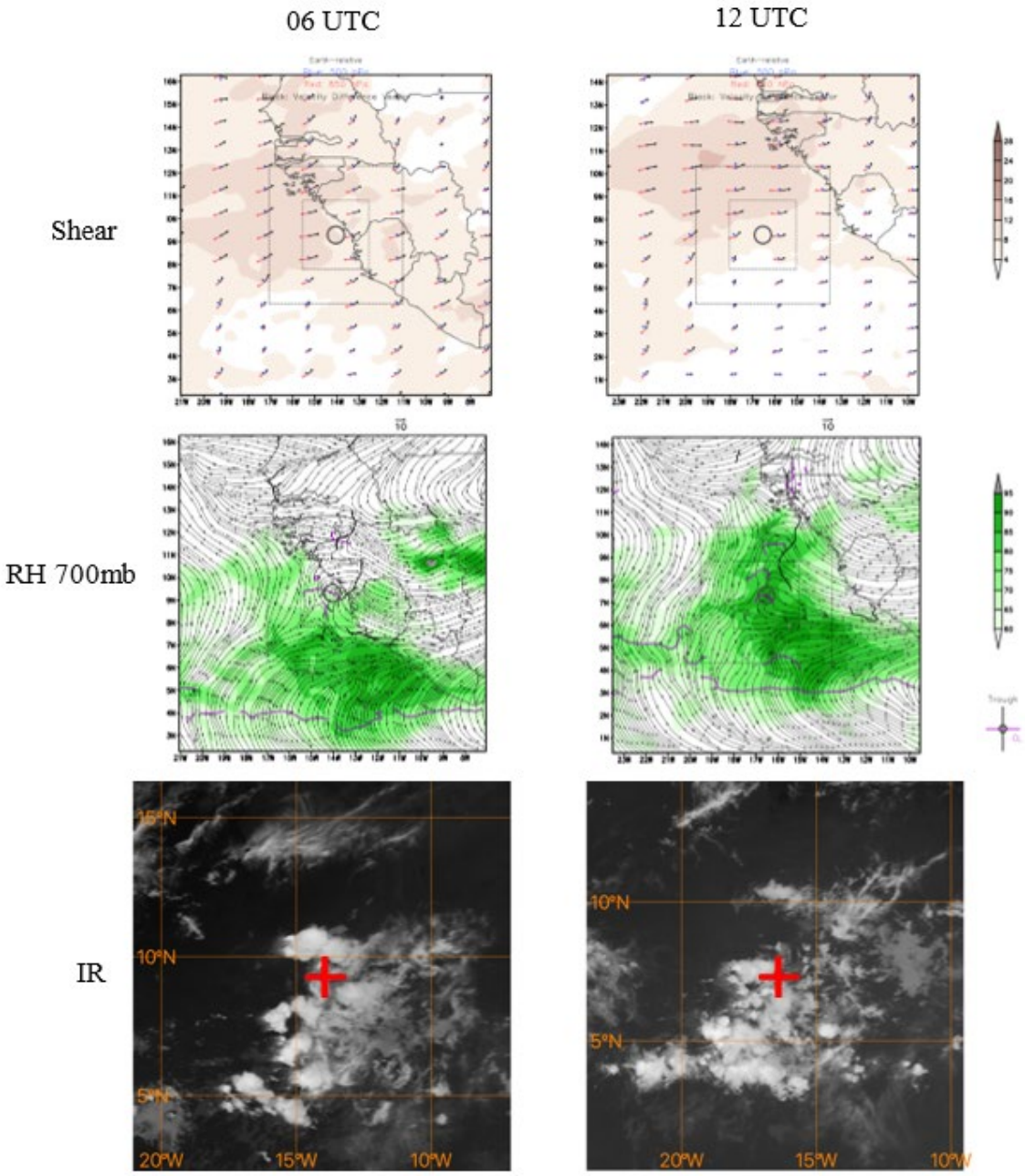

(Top row) GFS analysis of 500–850mb wind (note 10 m/s reference vector) and vertical wind shear (shading, m/s) at 06 UTC (left) and 12 UTC (right) 22 October. Blue arrows depict 500 mb wind, red arrows depict 850mb wind, and black arrows depict the difference between them. (Middle row) GFS analyses of 700 mb relative humidity (shading) and comoving streamlines at the same times. (Bottom row) Corresponding GOES-16 IR imagery, with the tracked circulation center denoted with a red plus at the image center.

Figure 10. Vertical Wind Shear, Relative Humidity, and IR 22 October 2020

1. Initial Pouch Formation

By 18 UTC 22 October 2020, a little more than 12 hours after leaving Africa, GFS depicted a developed pouch with 850 mb closed comoving streamlines around an area of positive OW (Figure 11, top left) and relative vorticity (Figure 11, top right). The streamlines were organized at the center of the pouch denoted by the trough (black line) and critical latitude (purple line) intersection. This 850 mb pouch was located on the northern edge of moist ITCZ air with 80% RH near the pouch center (Figure 11, bottom left). While the pouch was organized at the 850 mb level, for consistency, we continue to track the smaller and weaker 700 mb circulation at this time (not shown). The center of this smaller 700 mb circulation is denoted in (Figure 11) by the central circle, which was displaced about 1 degree (~60n. mi.) to the southwest of the 850 mb circulation center (Figure 11, top row, and bottom left).

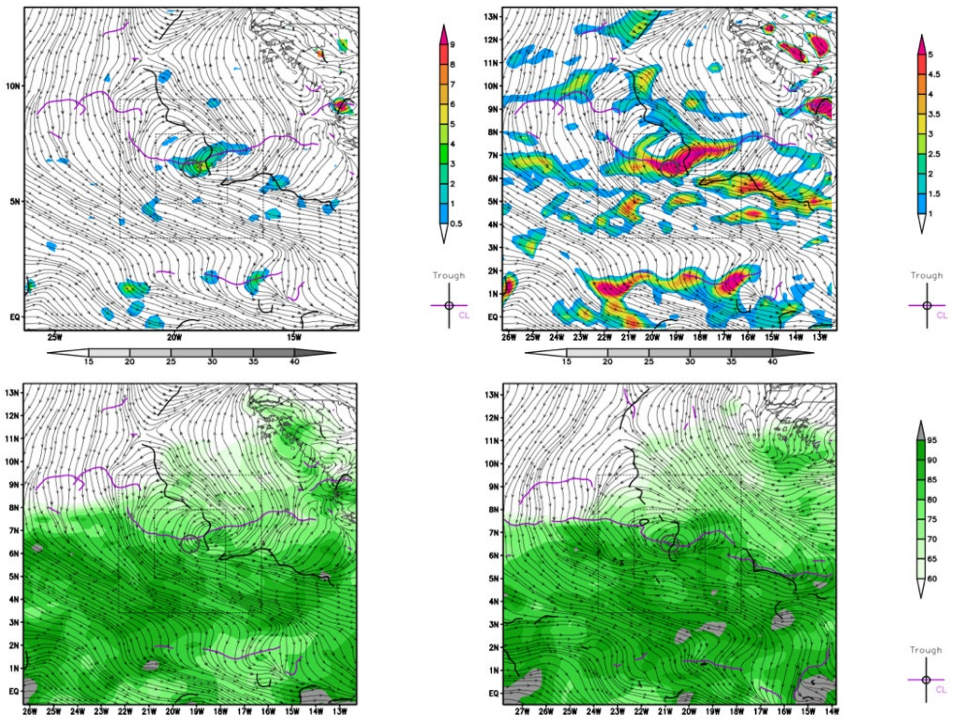

GFS 850-mb analyses with color shading of OW (top left) and relative vorticity (top right) with wind speeds (grey shading) and comoving streamlines at 18 UTC 22 October 2020. The corresponding GFS 850-mb analysis of RH (shading) and comoving streamlines is at the bottom left with the same type of plot 6 hours later at 00 UTC 23 October at bottom right.

Figure 11. Pouch Formation: OW, Vorticity, and RH

2. Instability Period

The Marsupial Paradigm states that one pathway for tropical cyclone formation can stem from local instability within the ITCZ: "Local instability of the ITCZ as a pathway to genesis is possible, although more commonly, the waves produced thereby propagate downstream into regions more favorable to genesis" (Dunkerton et al. 2009, pg. 5591). The climatological location of the ITCZ in October for this area in the Atlantic lies between 8–9°N (Žagar et al. 2011). During the analyzed instability section of our analysis, our pouch enters the ITCZ. Instability related to entering this zone leads to the formation of multiple circulations and OW maxima, which we analyze in some detail below since they play a role in the formation of the pouch that ultimately leads to the genesis of Hurricane Eta.

Six hours after initial pouch formation, at 00 UTC 23 October, the 850 mb RH values increased to 85% in the pouch center (Figure 12, middle right), and the 925 mb RH levels increased also (not shown). The circulation had become vertically aligned with the 700 mb position now only a few km west of the 850 mb pouch center (Figure 12, left). At this time a vorticity strip, a large horizontal region of positive relative vorticity, which had been gradually developing was detected in the 850mb level (Figure 12, bottom left). Before this, the relative vorticity was weaker, smaller in size, and did not exhibit the organization in the shape of a horizontal strip (Figure 11, top right and Figure 9, bottom).

After the formation of the vorticity strip, the disturbance system tracks westward with a small but consistent OW maximum at the 700 mb level and a much stronger OW maximum at 850 mb. We continued tracking at the 700 mb level for consistency. The OW at the lowest analyzed level, 925 mb (not shown), was very weak, sometimes disappearing completely from the analysis. This variation in lower-level intensity appears to be independent of diurnal convection patterns since the maximum analyzed convection and OW do not have any set pattern (not shown). This system was simply very weak at this time with a lot of instability.

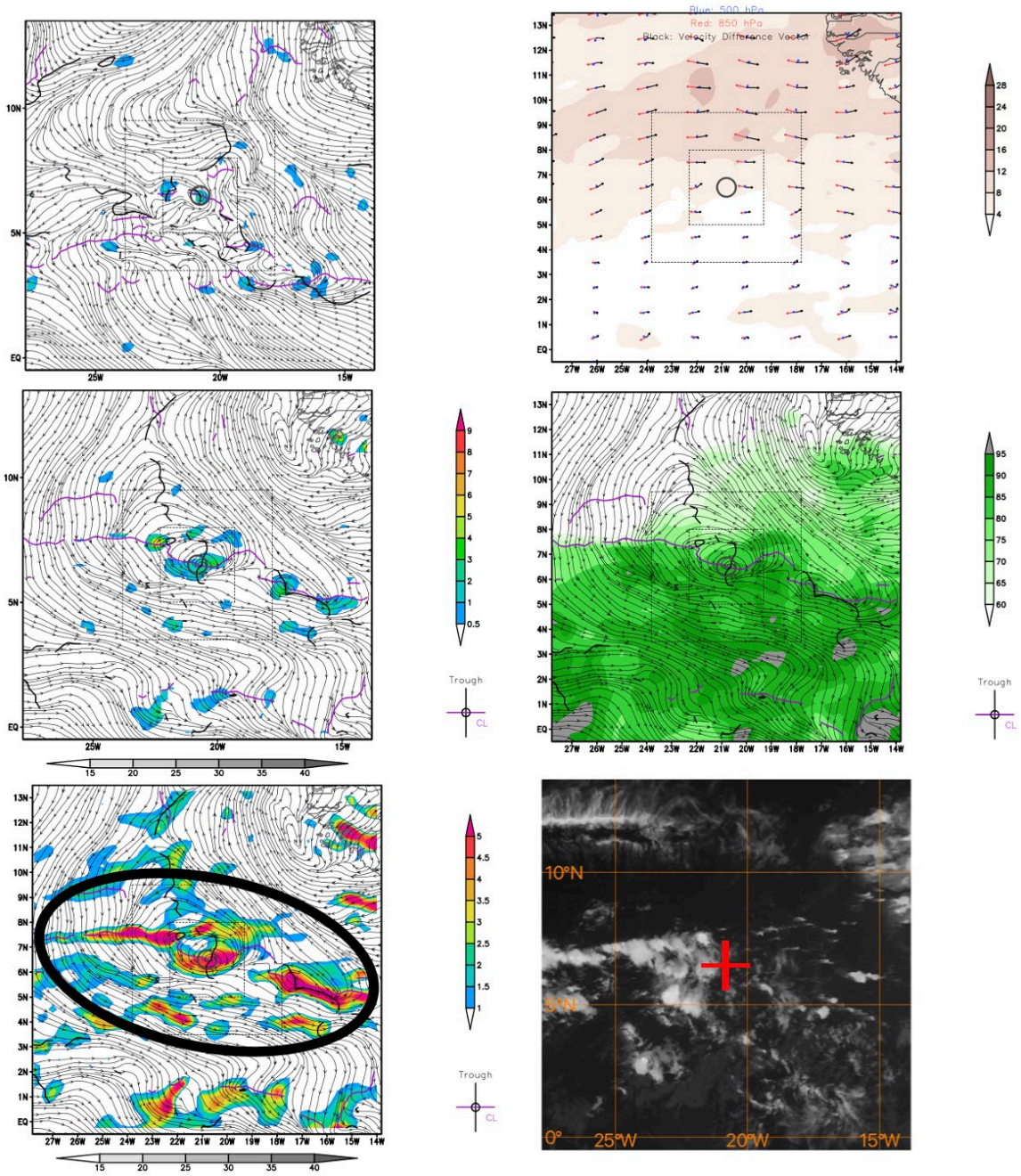

GFS 00 UTC 23 October analyses of comoving streamlines and wind speeds (grey shading) with color shading for OW at 700 mb (top left) and 850 mb (middle left), and 850 mb relative vorticity (bottom left) with a vorticity strip circled in solid black. 500–850 mb wind and vertical shear (shading, m/s) (top right), and 850 mb relative humidity (shading) and comoving streamlines (middle right). Corresponding GOES-16 IR imagery with red + at the center of the selected pouch center.

Figure 12. OW, Vorticity, Shear, and RH at 00 UTC 23 October 2020

Later that day, at 18 UTC 23 October, GFS depicted a vorticity strip down at the 925 mb level (not shown) that continued to strengthen, becoming strong by 00 UTC 24 October (Figure 13, bottom right). At this time, the GFS analysis depicted the closed circulation in the comoving frame had extended down to the 925 mb level. From these analyses, we infer that a deepening of the pouch occurred (Figure 13, bottom left).

At the time of the pouch deepening, 00 UTC 24 October, the system has a slightly tilted inverted conal shape. The center of circulation and OW at 700 mb is slightly west of the center of circulation in the OW and vorticity charts within the strongest pouch at 850 mb and 925 mb (Figure 13, left column). The vertical shear during this period is very weak between 500 and 850 mb levels (Figure 13, top right) and the RH is very high (Figure 13, middle right). IR imagery reveals that convection was widespread but weak and scattered at 00 UTC 24 October (Figure 14, left). However, by 18 UTC 24 October, convection is more concentrated near the location of the tracked 700 mb pouch center (Figure 14, middle and right).

Starting at 00 UTC 25 October, the tilt shifts in the opposite direction resulting in an eastward tilt with the two lower levels positioned west of the upper 700 mb level (Figure 15, left column). The trend of convection organizing near the pouch center continues as seen in the GOES-16 IR image (Figure 15, bottom right).

a. Intra-pouch Merger

At 00 UTC 25 October, the vorticity strip is very strong and extends northeastward from 5°N, 39°W to 12°N, 30°W (Figure 15, middle right). This high positive relative vorticity fed the formation of a secondary OW maximum within our pouch first detected at 06 UTC 25 October at 850 mb (8.73°N, 33.8°W) (not pictured). By 12 UTC 25 October two OW maxima are seen not only at 850 mb but down to the 925 mb level as well (Figure 16, bottom and middle left). The two OW maxima were mostly vertically aligned between 850 and 925 mb levels. The single 700 mb maximum was aligned with the eastern maximum.

AT 00 UTC 26 October the pouch weakens, and circulation is no longer visible in the 700 mb level, becoming shallower (Figure 16, top middle). This prompted us to start tracking the pouch at the 850 mb level.

The two OW maxima continue to strengthen until their peak OW at 06 UTC 26 October. The amount of convection did increase significantly during the 18 hours from when the second OW maxima emerged on 06 UTC 25 October (Figure 17, left) to immediately before the point of maximum strength where banding features are detected around the pouch (Figure 17, right). TPW charts in (Figure 4) also show the significant 24 hour increase in amount of precipitable water within the system from 25 October to 26 October. At 00 UTC 27 October, the two OW maxima merge creating an even larger single OW maxima (Figure 16, right column).

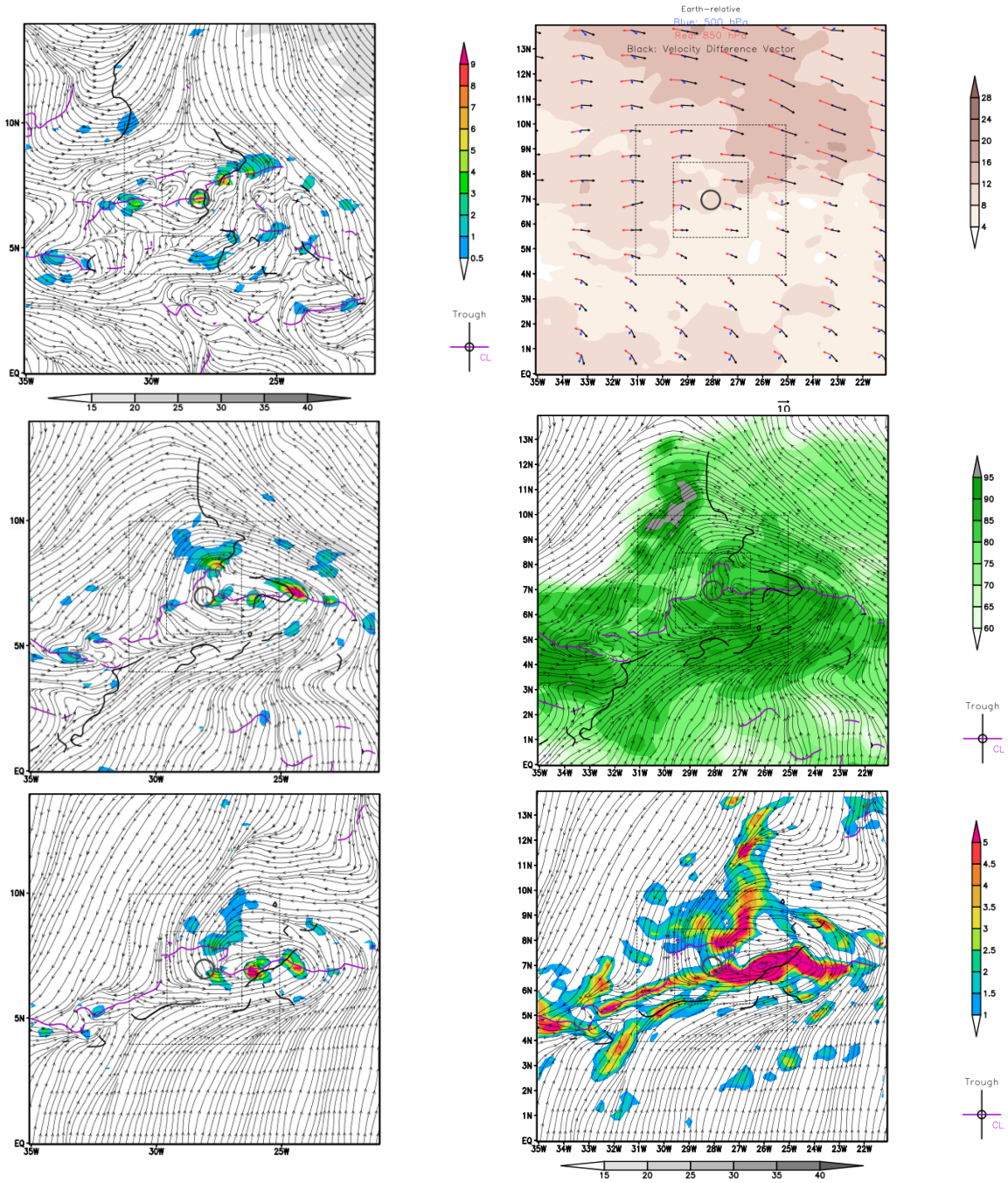

GFS 00 UTC 24 October analyses of comoving streamlines and wind speeds (grey shading) with color shading at 700 mb OW (top left), 850 mb (middle left), 925 mb (bottom left), relative vorticity at 925 mb (bottom right), 500–850 mb wind and vertical shear (shading, m/s) (top right), and 850 mb relative humidity (shading) and comoving streamlines (middle right).

Figure 13. Vertical Tilt at 24 October 00 UTC

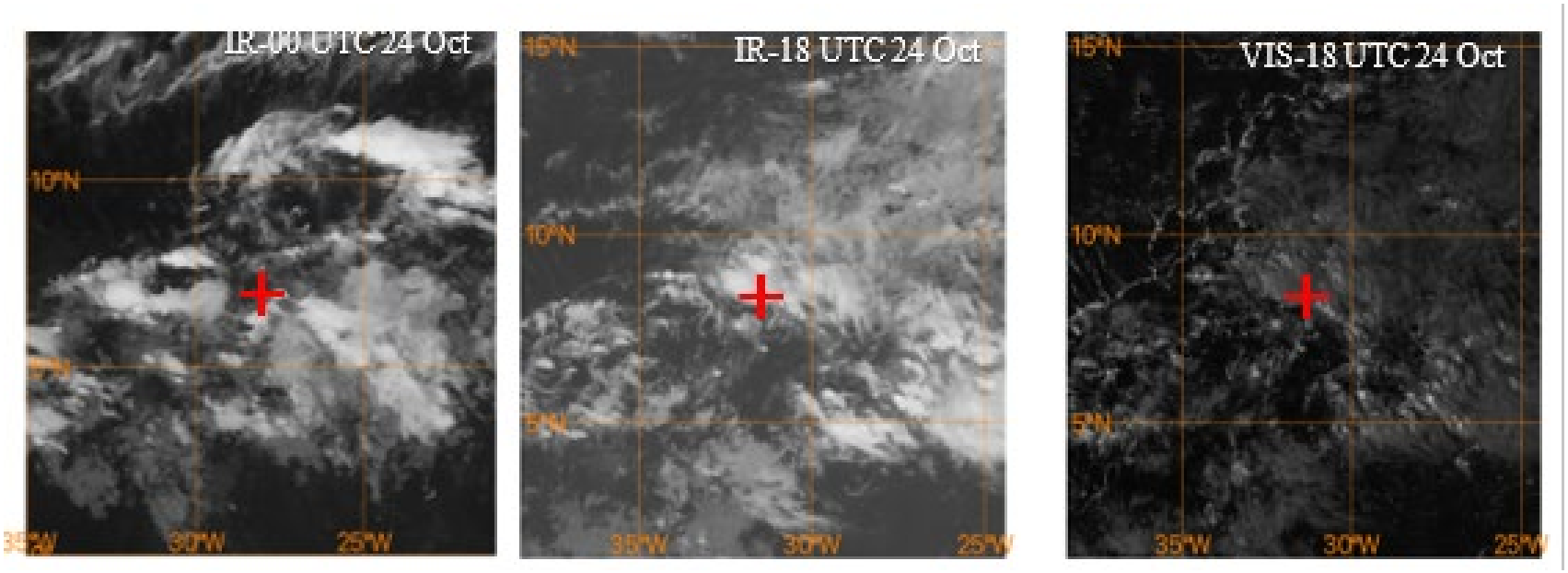

GOES-16 IR imagery at 00 UTC (left) and 18 UTC (middle). GOES visible imagery at 18 UTC (right) 24 October. The red + denotes the selected pouch center.

Figure 14. IR and Visible Imagery 24 October 2020

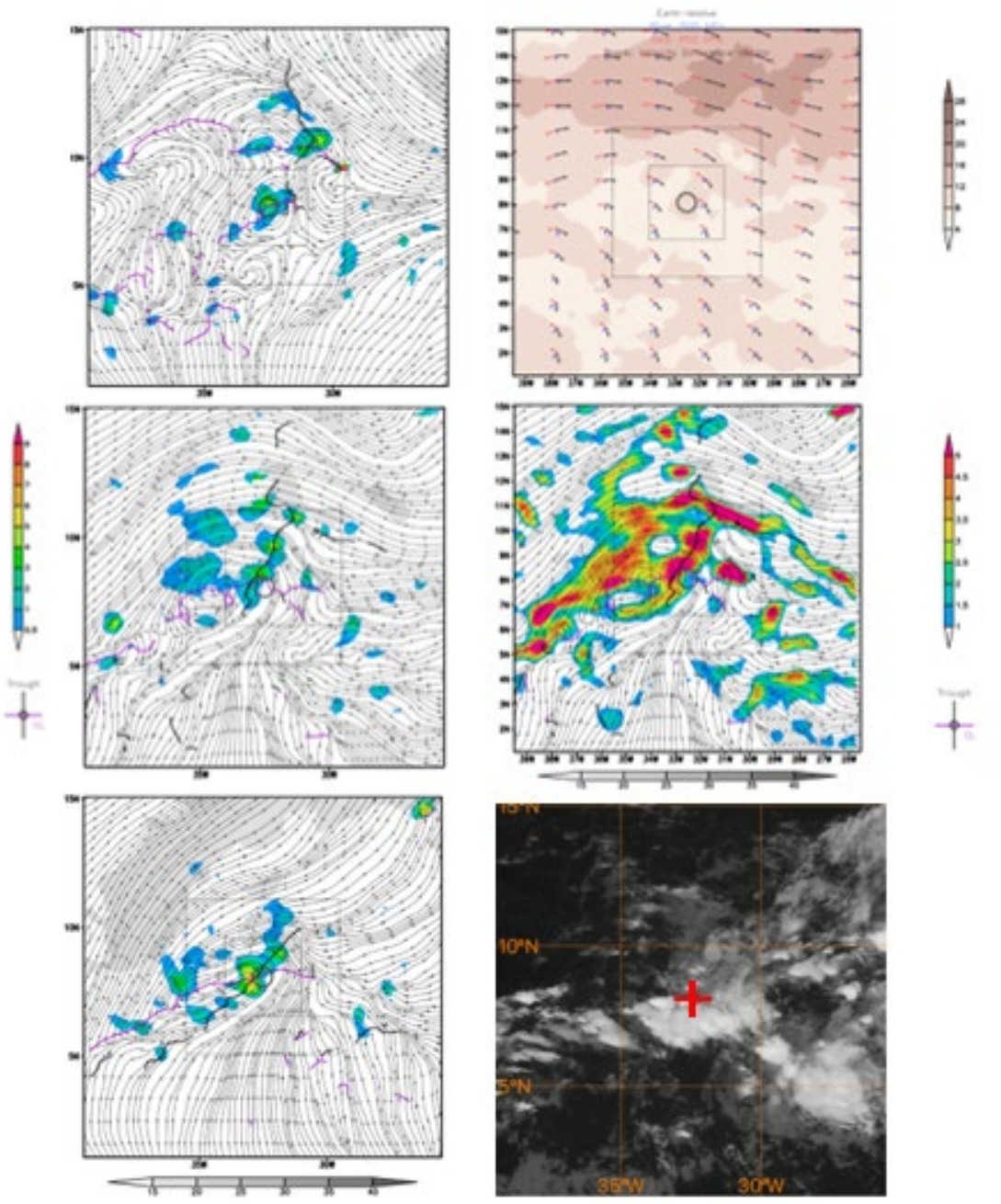

GFS 00 UTC 25 October analyses of comoving streamlines and wind speeds (grey shading) overlaid with color shading at 700 mb OW (top left), 850 mb (middle left), 925 mb (bottom left), relative vorticity at 850 mb (middle right), 500–850 mb wind and vertical shear (shading, m/s) (top right). Corresponding GOES-16 IR imagery is at the bottom right with the red + at the pouch center.

Figure 15. 25 October 2020; OW, IR, Wind Shear, Relative Vorticity

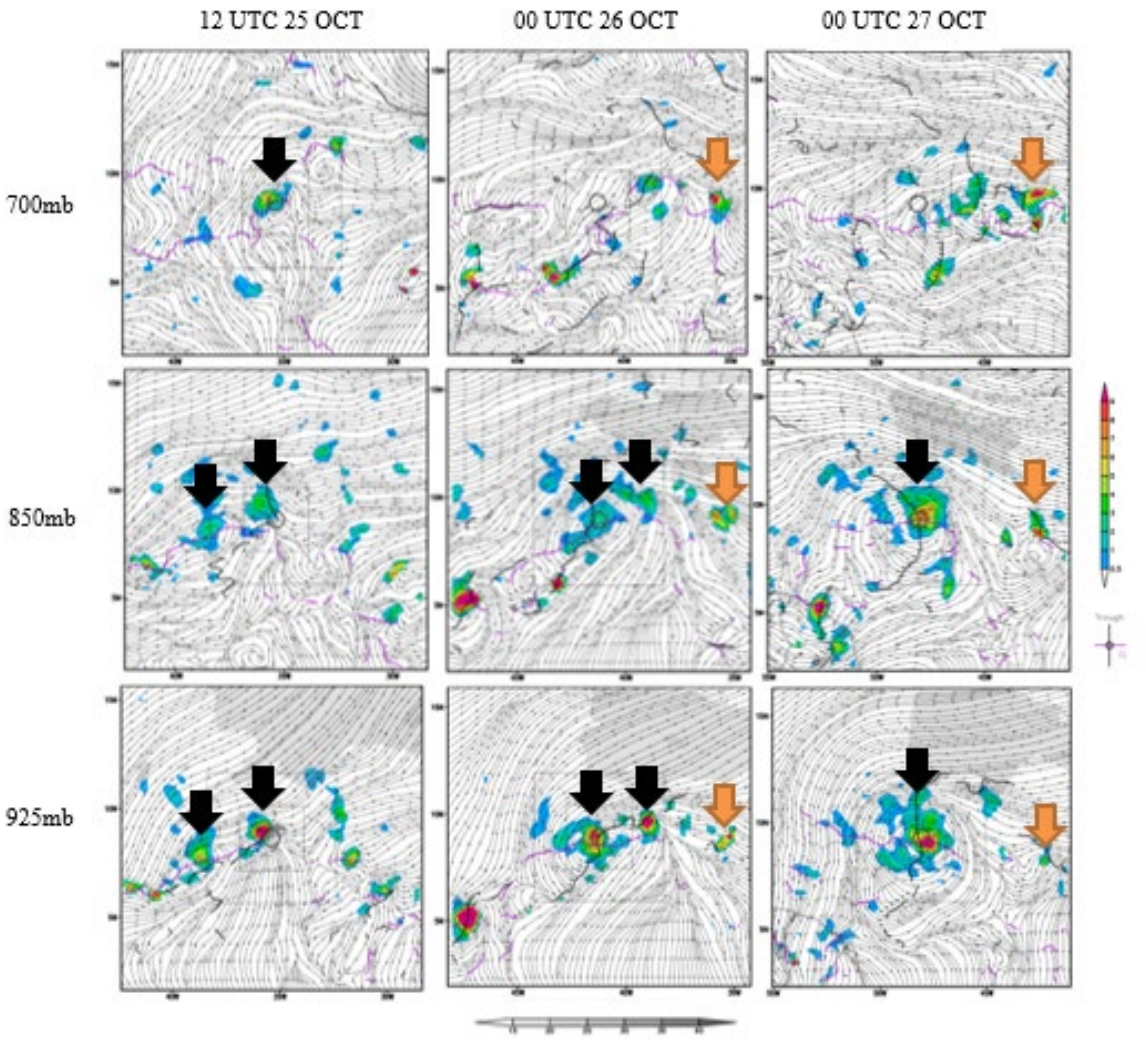

GFS analyses of OW (color shading) overlaid with comoving streamlines and wind speeds (grey shading) at; 700 mb (top), 850 mb (middle), and 925 mb (bottom) at 12 UTC 25 October (left), 00 UTC 26 October (middle), and 00 UTC 27 October (right). The black arrows denote the OW maxima within the original pouch. The orange arrows mark the secondary OW maxima outside the pouch which later dissipated.

Figure 16. OW Maxima Merge

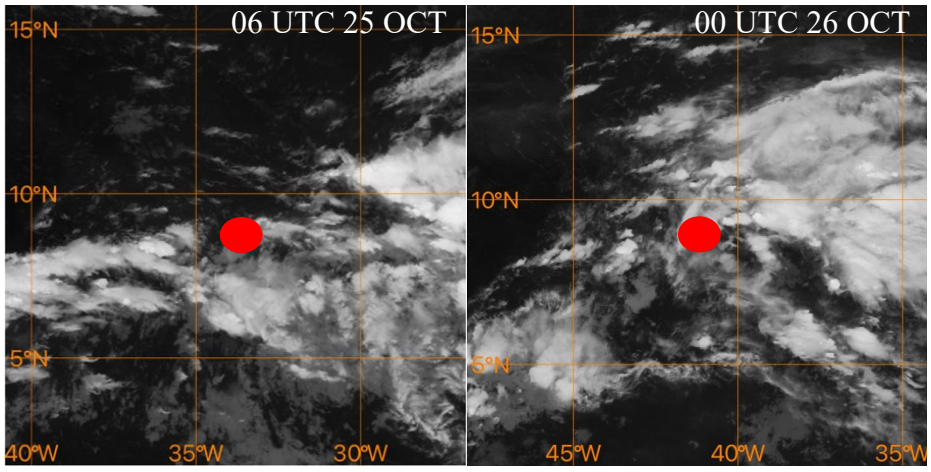

GOES-16 IR imagery at 06 UTC 25 October (left) and 00 UTC 26 October (right) The red dot is the center of the selected pouch.

Figure 17. 25 October 2020 IR Imagery

b. New Circulation Emerges/ Pouch Shallowing

There was a second notable phenomenon that emerged during the period just analyzed. At 00 UTC 26 October, the same time as the shallowing of the pouch, a secondary circulation develops outside and to the east of our pouch (Figure 16, middle column with orange arrows). This circulation arises from the midsection of the broken vorticity strip. This secondary OW maximum is much reduced in magnitude than our pouch's OW and is part of an open wave instead of a closed circulation. This secondary OW maximum intensifies, especially at 700 mb, by 00 UTC 27 October (Figure 16, right). It has atmospheric depth, and it is detected to stretch out from 700 mb down to 925 mb, although it is much weaker at the lower levels. This secondary OW maximum persists with high OW and moves along with our pouch until it dissipates on 18 UTC 27 October (not shown). We may attribute the rise of this circulation as the reason our pouch weakened.

First introduced in Figure 6, the pouch-centered 3° x 3° and 6° x 6° box averaged values of variables from the GFS analysis provide a summary of the first five days of Eta's precursor over the eastern Atlantic. During the initial pouch development stage from 06 to 12 UTC 22 October, relative humidity and equivalent potential temperature at the pouch-tracked level of 700 mb rapidly increased as the tracked disturbance system approached

the ITCZ (Figure 18, top right). In time-height plots of 3° x 3° box average values, positive mass flux, which provides a depiction of upward motion (Figure 19, left), and moist air indicated by high RH values (Figure 19, right) is limited to the lower 600 mb of the atmosphere on 22 October. On this first day, low values of OW and relative vorticity at the 700 mb tracked level (Figure 18, top left) are revealed by both the 3° x 3° and 6° x 6° box average time-height plots to extend throughout the atmosphere (not shown). The vertical shear analysis shows relatively low values of low-level pouch shear (between 5–7 m/s), and moderate deep shear (between 10–15 m/s) (Figure 18, bottom right).

During the period of instability and after the development of the pouch, between 00 UTC 23 October and 06 UTC 27 October, we detected an increase in the upward mass flux of our system in the time-height plot (Figure 19, left) which extended vertically from 1000 mb to almost 200 mb in both the 3° x 3° (Figure 19, left) and 6° x 6° (not shown) pouch-centered boxes. This mass flux went through periods of pulsing that can be associated with the stochastic deep convection located within the ITCZ area of instability (Figure 18, bottom left). The ebb and flow can be identified in the time-series plot with peaks on 22, 23, 25, and 26 October, (Figure 18, bottom left). Equivalent potential temperature and relative humidity (Figure 18, top right) also showed some pulsing with distinctive peaks on 22, 23, 25, and 27 October, but overall, both experienced a gradual increase. While RH values varied in vertical depth because of the associated ebb and flow, it had its biggest vertical extension during 23 October when the GFS detected extremely saturated air up to 200 mb in the 3° x 3° box (Figure 19, right). The OW and relative vorticity values remained relatively low at the beginning of this period, but relative vorticity modestly increased on 26 October at the time of the tracked level transition from 700 mb to 850 mb (Figure 18, top, left). The time-height plot (not shown) reveals that positive OW values are confined to below the 700 mb level and positive relative vorticity values to below 600 mb. The pouch shear stays relatively low, never going higher than about 8 m s^{-1}, while the deep shear increases to a maximum of about 15 m s^{-1} at the end of 25 October (Figure 18, bottom right). Both pouch and deep shear also showed some pulsing with distinctive peaks in shear on 23, 25, and 27 October.

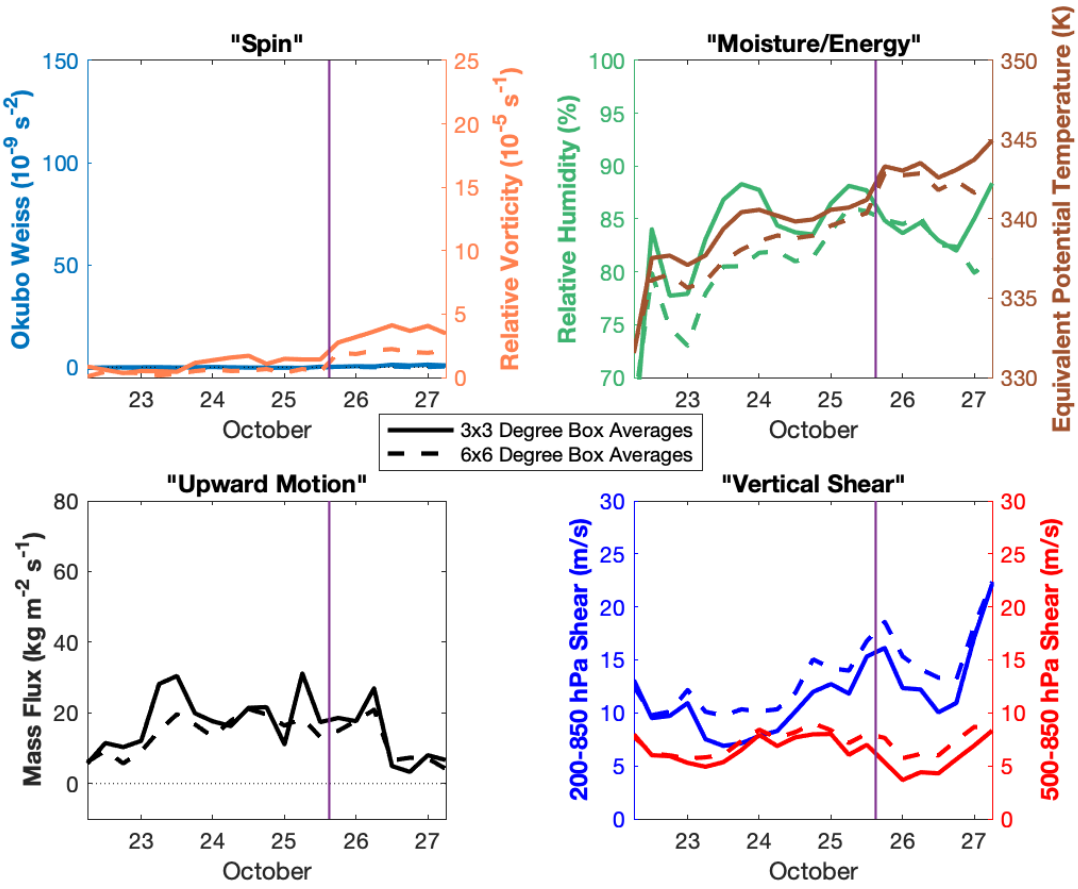

Time series of GFS analysis pouch-centered 3° x 3° (solid) and 6° x 6° (dashed) box average values (see boxes in Figure 6) of seven variables during 06 UTC 22 October to 06 UTC 27 October: OW (top left, blue line), relative vorticity (top left, orange line), RH (top right, green line), equivalent potential temperature (top right, brown line), mass flux (bottom left), low level 500–850 mb vertical wind shear (bottom right, red line), and deep 200–850 mb shear (bottom right, blue line). Values are calculated at the level at which the pouch is tracked (700 mb until 12 UTC 25 October before purple vertical line, 850 mb thereafter).

Figure 18. Time Series 22 –27 October 2020

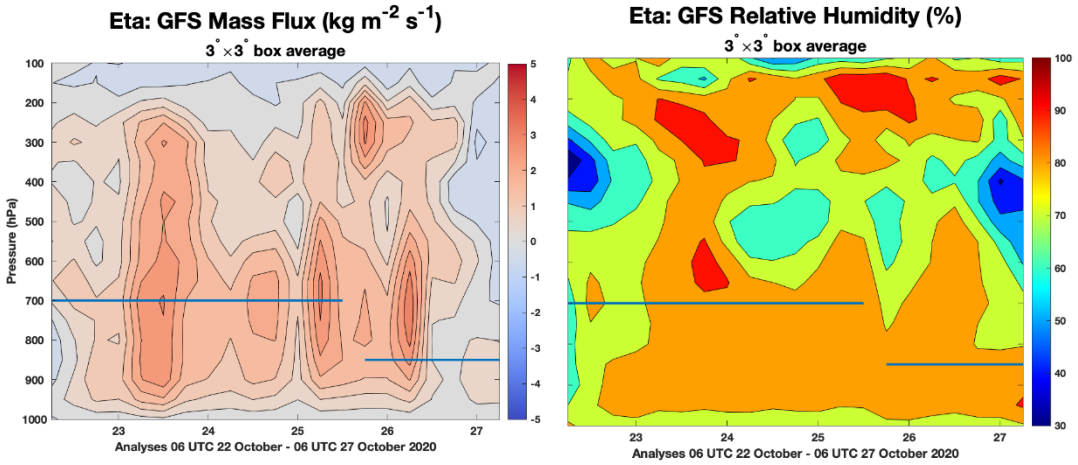

GFS time versus height analysis of mass flux (left) and relative humidity (right) in the 3° x 3° pouch-centered box, from 06 UTC 22 October to 06 UTC 27 October. The vertical axis represents pressure levels of GFS output that had 50-mb increments. The blue horizontal line represents the pressure level used to track the system (700 mb through 12 UTC 25 October, 850 mb thereafter).

Figure 19. Mass Flux and RH 22–27 October 2020

B. MIDDLE PHASE

1. Secondary Pouch Formation

At 12 UTC 27 October, when the pouch was at 9.69N, 51.20W (left/west edge of Figure 20 panels), a second OW maximum and convective center emerged and strengthened further east at -7.8N, 44.55W (Figure 20, center of top left). This new OW maximum emerges from the end of the previously mentioned vorticity strip following a rollup of the vorticity, which has been noted before (Figure 20, bottom left).

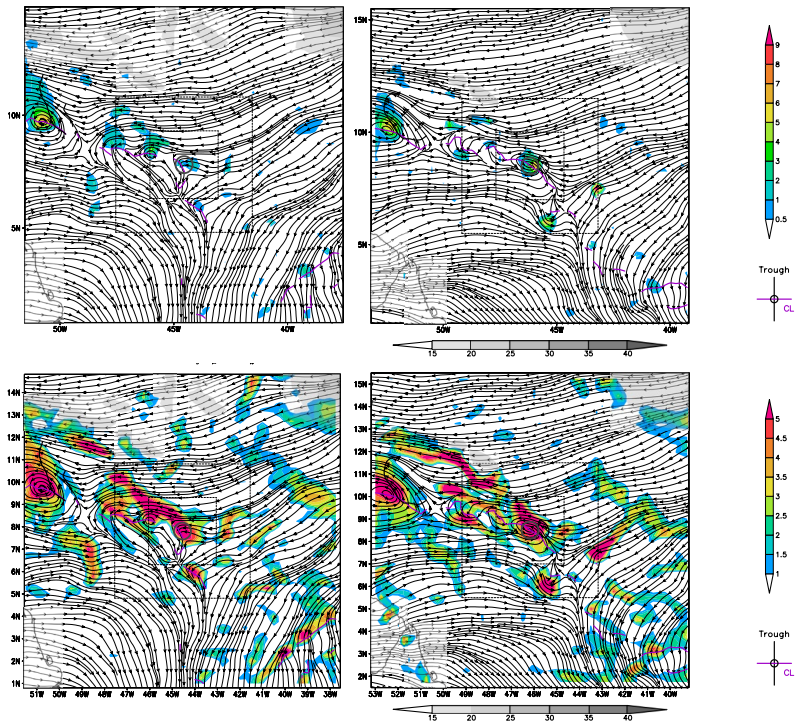

GFS 27 October analyses of comoving streamlines and wind speeds (grey shading) with color shading at 12 UTC of 850 mb OW (top left) and relative vorticity (bottom left). The right column depicts the same variables at 18 UTC.

Figure 20. OW and Vorticity 27 October 2020

In our next analyzed period, 6 hours later at 18 UTC 27 October, there is a noticeable increase in OW for our new maximum (Figure 20, top right). At this time, this new OW maximum begins to have a quasi-closed circulation. This denotes the formation of a new pouch which we will now call the eastern pouch. The original pouch we have been tracking since its formation near Western Africa will now be called the western pouch. During the development and strengthening of the eastern pouch between 12 and 18 UTC 27 October, increasing convection is detected above the eastern pouch (Figure 21).

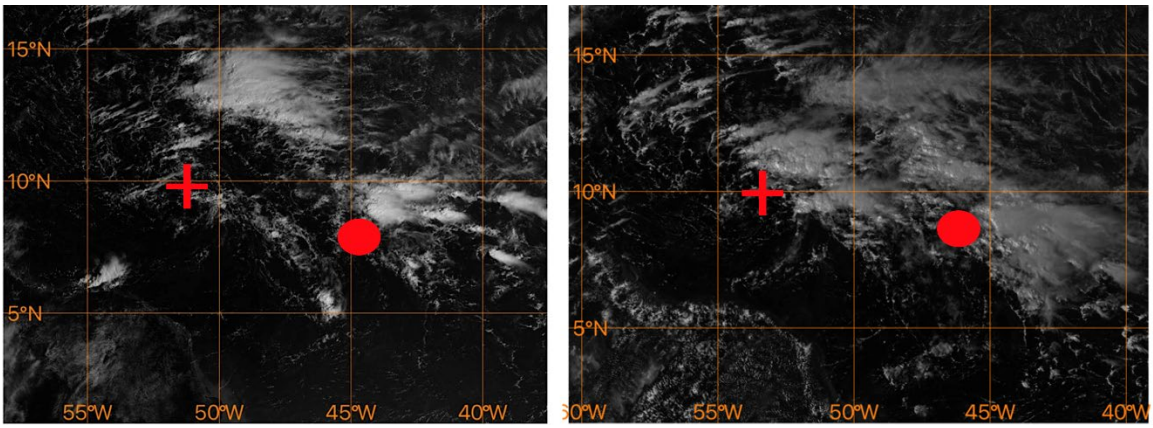

GOES visible imagery 27 October 12 UTC (left) and 18 UTC (right). The red + is the center of OW for the western pouch and the red dot is the center of OW for the eastern pouch.

Figure 21. Visible Imagery 27 October 2020

Convection became noticeably stronger above the eastern pouch than the western pouch as time progressed (Figure 21). Circulation and strong pockets of convection are visible over the easter pouch in the IR image at 00 UTC 28 October (Figure 22, left). At 06 UTC 28 October, there is a strong singular convective center over the eastern pouch, with minimal convection near the western pouch (Figure 21, right). The eastern pouch is smaller in horizontal extent than the western pouch but has about the same OW maximum. Another thing to note is that the eastern pouch has a greater vertical extent than the western pouch, and it is starting to develop a circulation at the 700 mb level, which explains the visible convection over the pouch.

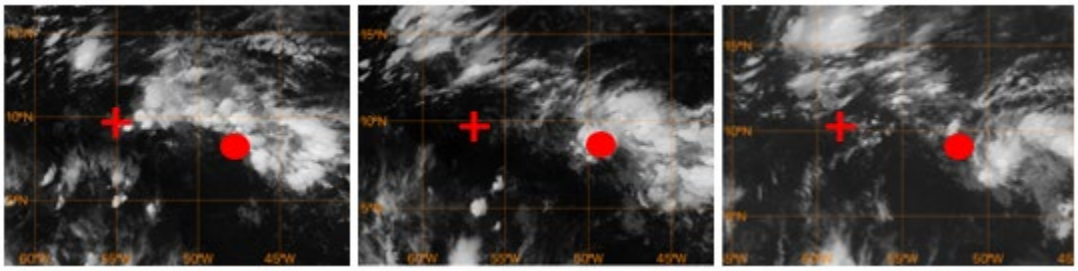

GOES-16 IR imagery 28 October at 00 UTC (left), 06 UTC (middle), and 12 UTC (right). The red + is the center of OW for the western pouch and the red dot is the center of OW for the eastern pouch.

Figure 22. IR Imagery 28 October 2020

At 12 UTC 28 October (not shown) the eastern pouch developed higher values of OW than the western pouch, and this property is found throughout a deeper layer. At this time a closed circulation for the eastern pouch can be seen throughout the analyzed atmosphere from 925 mb to 700 mb, whereas the western pouch still only has circulation from 850 to 925 mb. The eastern pouch is rapidly deepening, and convection is still mostly seen above the eastern pouch, with less convection associated with the western pouch (Figure 22, right).

2. Pouch Merger

The two pouches, eastern and western, have individual circulations and are over 7.3 degrees from each other at their furthest separation period at 06 UTC 28 October. After this maximum separation, the two pouches began approaching each other, still having individual circulations. The 850 mb co-moving analysis at 12 UTC 28 October (Figure 23, left column) indicated there was a saddle point between the two pouches at 9.5N, 54W. The saddle point represents a point in the flow where the airflow between the two pouches cannot easily flow between them and serves to isolate each pouch from the other. By 18 UTC 28 October the saddle point dissipated, (Figure 23, middle column). While the saddle point disappears, the two pouches begin interacting with each other, and the distance between the two OW centers is about six degrees. The two convective centers associated with each pouch can be seen in Figure 24 (left panel). The interaction between the two pouches forces the two circulations to become one large circulation, effectively a single pouch with two massive OW centers at 00 UTC 29 October. Figure 24 (middle) shows the IR imagery of this event, and Figure 23 (right column) shows the OW and streamlines during the same time. It is around this time when OW was finally detected at 700 mb above what was the western pouch.

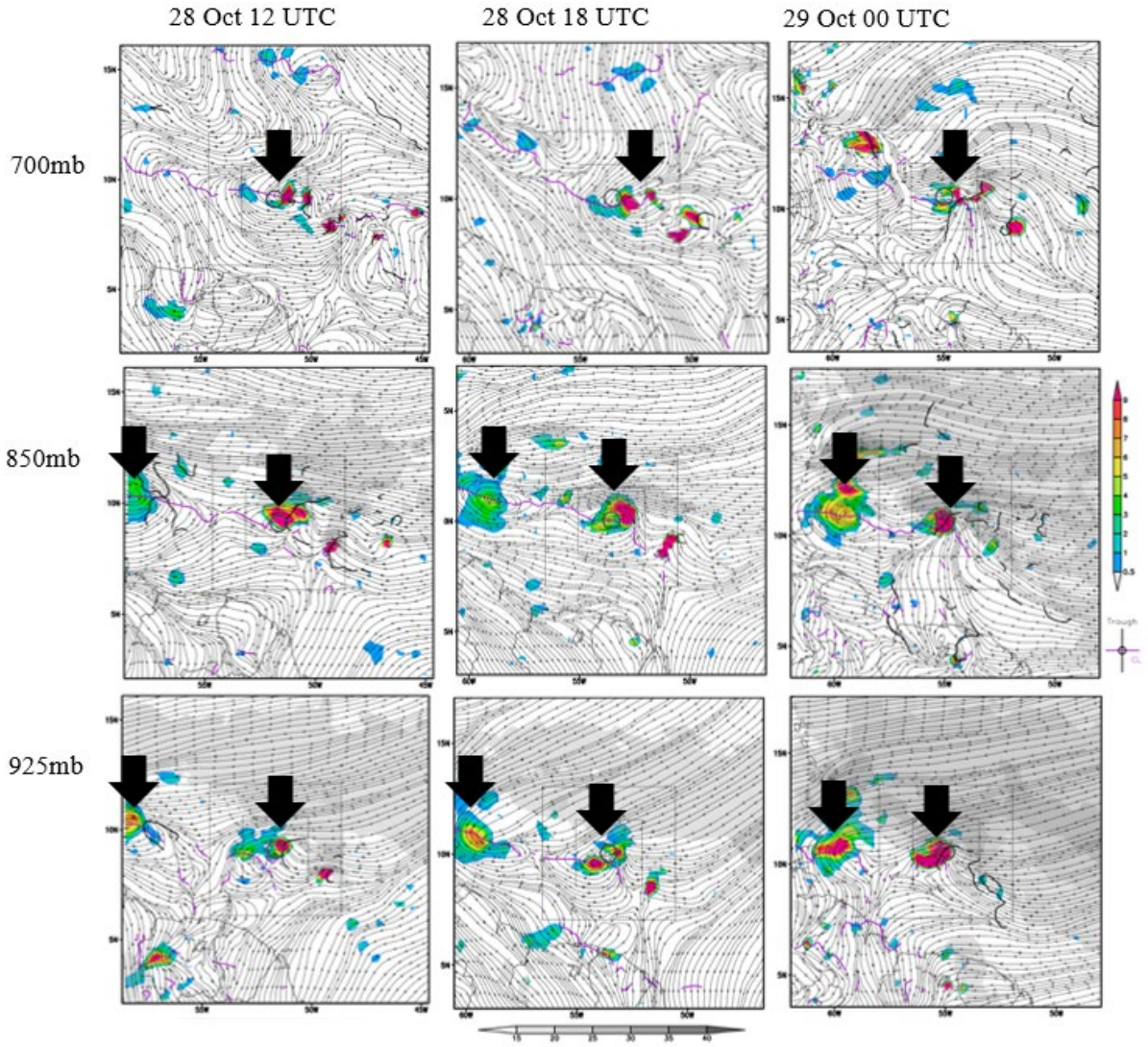

GFS analyses of comoving streamlines, wind speeds (grey shading) and OW (color shading) at 700, 850, and 925 mb (top to bottom respectively) at 12 UTC 28 October (left column), 18 UTC 28 October (middle column), and 00 UTC 29 October (right column). Panels are centered on the eastern pouch, with each pouch highlighted by a large black arrow.

Figure 23. OW 28 October and 29 October 2020 (eastern pouch)

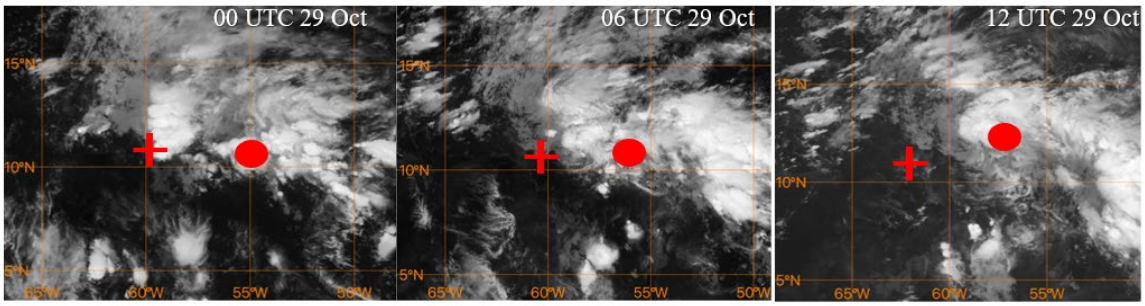

GOES-16 IR imagery 00 UTC 29 October (left), 06 UTC 29 October (middle), and 12 UTC 29 October (right). The red + is the center of OW for the western pouch and the red dot is the center of OW for the eastern pouch.

Figure 24. IR Merger Period during 28–29 October 2020

The eastern circulation's flow advects the western maxima toward it, showing direct cyclone interaction behavior (Carr et al., 1997). At 00 UTC 29 October, the two circulations are completely overlapping (Figure 23, right column). The western maximum sharply slows down, and the eastern maximum also slows down but not as much as the western maxima; see OW, vorticity, and satellite imagery (Figure 23, right column and Figure 24, left). This near-immediate change in phase speed is further evidence of this interaction which can be classified as a mutual cyclone interaction since the circulation of both appear to advect each other. In this case, the interaction is asymmetrical since the larger circulation from the eastern pouch has more effect than the smaller circulation associated with the western pouch. The merging of the two OW maxima finally ends at 06 UTC 30 October. At this time, one singular, massive OW maximum within the single pouch is detected. The resulting pouch with its OW maximum is Eta's precursor. This merger can be seen in OW, vorticity (not shown), and satellite imagery (Figure 25, right).

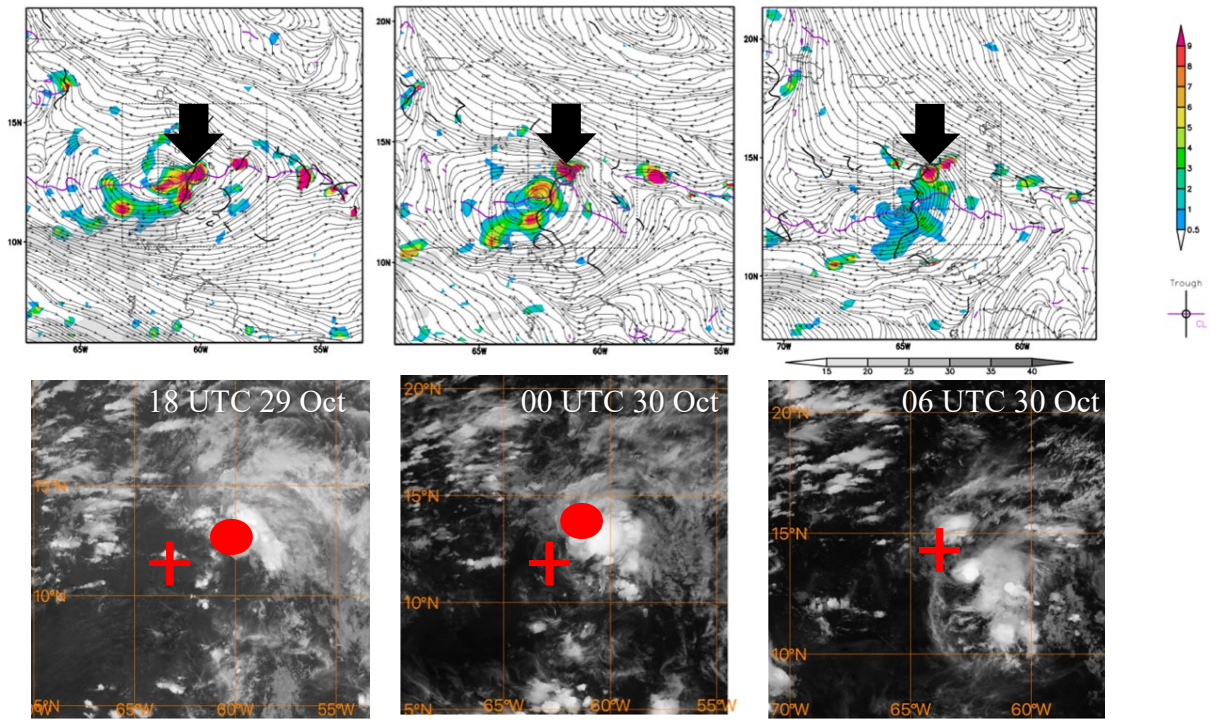

GFS analyses of comoving streamlines, wind speeds (grey shading), and OW (color shading) at 18 UTC 29 October (top left), 00 UTC 30 October (top middle), and 06 UTC 30 October (top right). Corresponding GOES-16 IR imagery is in the bottom row. The red + is the center of OW for the western pouch and the red dot is the center of OW for the eastern pouch.

Figure 25. End of Merger 29–30 October 2020

The merger of the pouches yielded a large, but not completely organized, system now located in the eastern Caribbean characterized by high SST values. From 06 UTC 30 October to 12 UTC 31 October, the system organizes, experiences curved band features, and approaches alignment throughout the atmosphere (Pasch et al. 2021). At 12 UTC 30 October we can see this near-aligned system in Figure 26, left column. Also, around this time, the vorticity strip finishes getting wrapped around the pouch center (not shown). The RH during the 2020 season was especially high west of 70°W and, our system crossed that threshold between 06 and 12 UTC 31 October (Klotzbach et al. 2021). A closer and more organized system with almost perfect vertical alignment is seen at 18 UTC 31 October (Figure 26, right column), when the NHC classifies the system as a Tropical Depression. Satellite imagery also depicts the organization of the system (Figure 27). The system is located about 190 n. mi. south of Pedernales, Dominican Republic (Pasch et al. 2021).

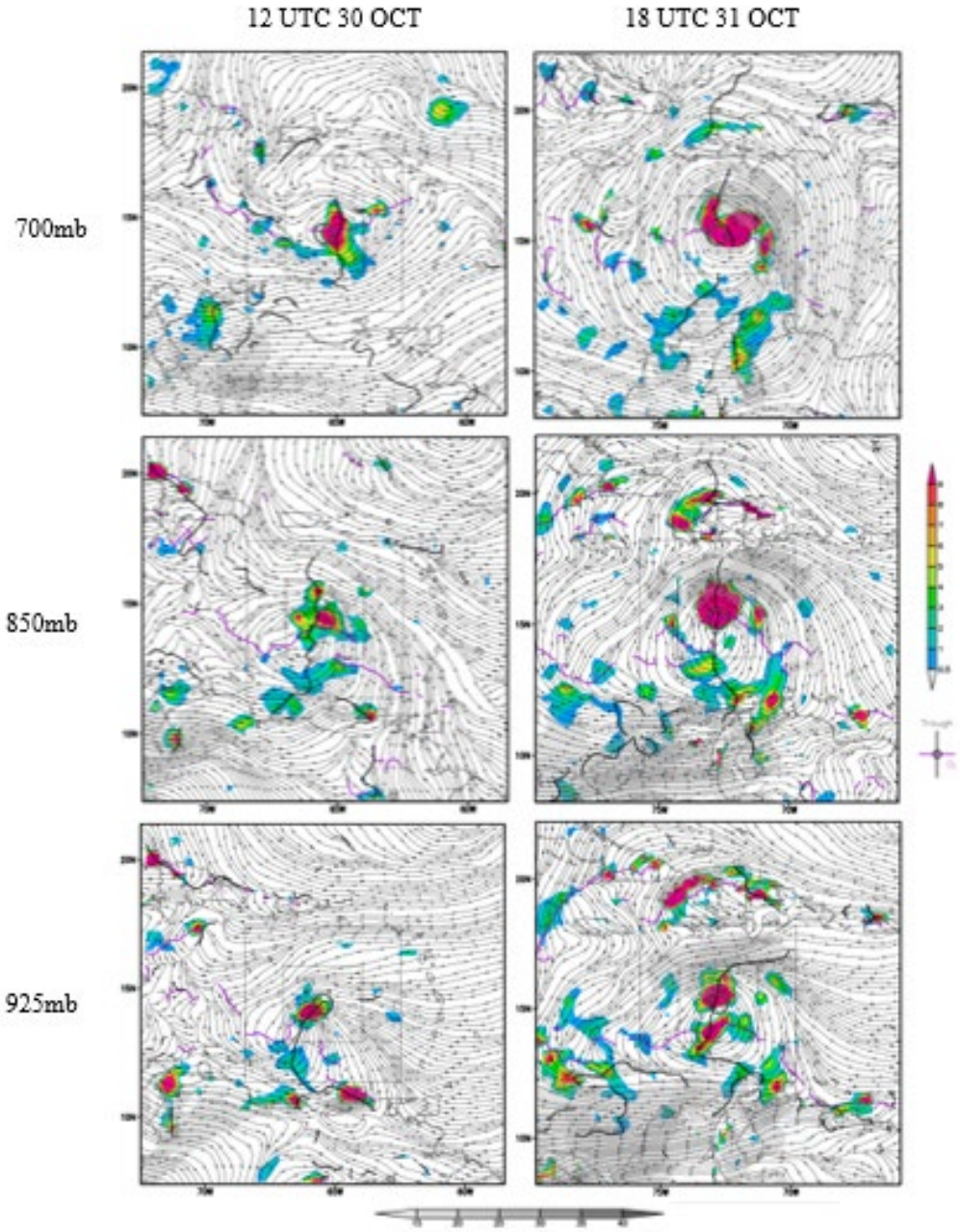

GFS analyses of comoving streamlines, wind speeds (grey shading), and OW (color shading) at 700, 850, and 925 mb (top to bottom respectively) at 12 UTC 30 October (left column) and 18 UTC 31 October (right column).

Figure 26. OW Vertical Alignment of TD during 30–31 October 2020

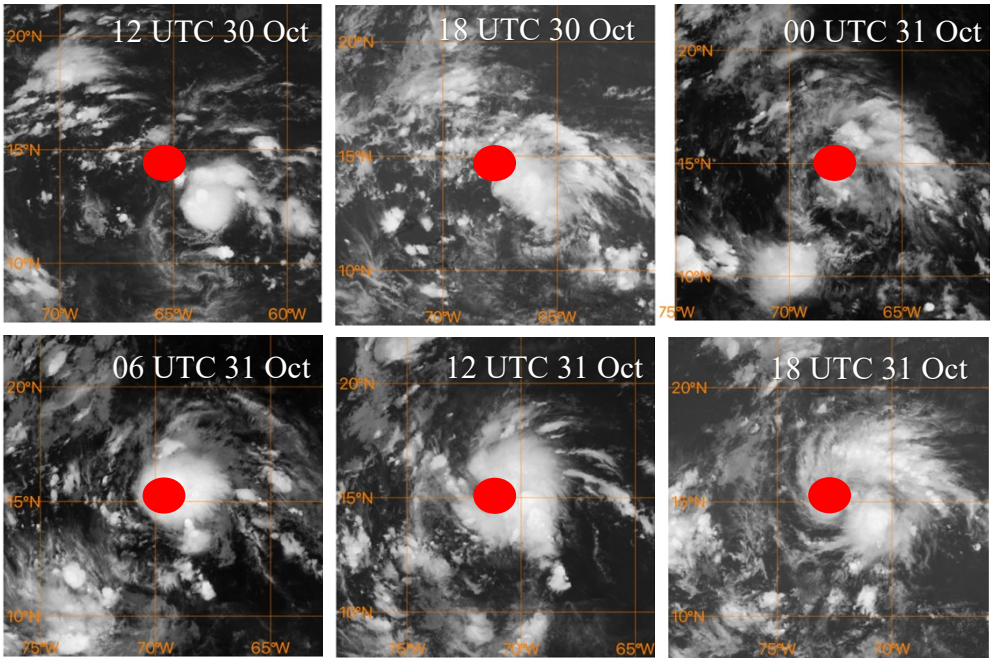

GOES-16 IR imagery at 12 UTC 30 October (top left), 18 UTC 30 October (top middle), 00 UTC 31 October (top right), 06 UTC 31 October (bottom left), 12 UTC 31 October (bottom middle), and 18 UTC 31 October (bottom right). The red + is the center of OW for the pouch.

Figure 27. IR Imagery 30 October and 31 October 2020

In summary, the newer eastern pouch had about the same OW throughout the troposphere as the western pouch from its emergence until the saddle point disappeared at 18 UTC 28 October. After this point, the eastern pouch had an increase of OW from 600 mb down to 1000 mb. At this time, there was also an intense increase in vertical mass flux, which extended between 100 mb to 1000 mb. This was the beginning of the merger. The western pouch was much shallower than the eastern pouch, extending from about 400 mb to 950 mb. This lack of vertical depth in the western pouch when compared to the eastern pouch can explain why convection was mostly detected over the eastern pouch during the entire two-pouch analysis. The western pouch had slightly higher OW before the merger in the lower troposphere from 700–1000 mb. After the saddle point disappeared, the western pouch increased vertical mass flux, but it was still slightly weaker than the eastern pouch's mass flux at the same time.

The relative vorticity for the eastern pouch was high between 600–1000 mb for most of the period where we detected two separate pouches and up to 300 mb during the mass flux period. In contrast, the relative vorticity for the western pouch was high in a limited area of the troposphere, between 800–1000 mb. The western pouch maintains steady relative vorticity in the lower troposphere for most of the period until the merger when relative vorticity rapidly increased in the upper levels, which can be attributed to the contribution by the eastern pouch. The pouch shear for both pouches during the entire period was relatively low (less than 10 m s^{-1}). Although the deep shear for the western pouch increased to a peak of about 25 m/s right before the saddle point broke, this high shear was likely caused by the closer interaction with the eastern pouch right before the merger. This deep shear decreased rapidly after the saddle point broke at 18 UTC 28 October, and during the merger process.

We found that the eastern pouch had high relative humidity in the 3° x 3° box throughout the entire two pouch timeline. RH ranged between 80–95% from 500 mb to 1000 mb. However, there was a notable dry patch of air during 28–29 October, with RH values between 40–65% at 200–500 mb. This patch of dry air recedes from our analysis window after the saddle point disappears and the two systems start merging, leading to near saturation from 150 mb down to 1000 mb.

The 6° x 6° box showed slightly lower RH overall because the convection was located closer to the pouch's center. The dry patch of air previously mentioned can be seen until the end of the two-pouch period for the same reason mentioned above. The western pouch had low relative humidity, 30–60% RH in the mid to upper troposphere (100-800 mb) when looking at the 6° x 6° box. The western pouch had a higher RH, 80–90%, between 850 mb to about 1000 mb. At the end of this period, while the two pouches are merging, another dry patch of air is evident in the eastern pouch's 6° x 6° and 3° x 3° box averages. This dryer air is most notable on the 6° x 6° box, which is why it is most likely associated with the dryer air being advected from the western pouch as they are in very close proximity. This dry air was only temporary and ultimately did not affect the development of the evolving larger moist system. The equivalent potential temperature is much higher in the eastern pouch than the western pouch throughout the entire period,

following the same trends as the RH. The eastern pouch shows higher theta-e or moisture content and relative humidity, which explains the detected higher convection for this pouch than the western pouch.

After the pouches merged into a single pouch, from 06 UTC 31 October to 12 UTC 31 October, there was a progressive increase of relative vorticity, relative humidity, and equivalent potential temperature right before the system was declared a TD. There was also a noticeable increase in vertical mass flux and OW for the single pouch between 500–1000 mb. While the pouches merged, we saw supporting evidence with the increased shear of the western pouch and the dry air in the upper atmosphere as the eastern pouch advected the western pouch. Ultimately, the two pouches fused into one larger-scale pouch circulation, and the circulation and convective activity were on the brink of becoming a tropical depression.

C. FINAL PHASE

As we have discussed, the initial phase of our system included the initial wave leaving Africa, the formation and deepening of the initial pouch, and an intra-pouch merger event. The Second or Middle Phase included the formation of the eastern pouch and the merger process with the original or western pouch. This merger process was a catalyst to the final phase, the progression of the system into a TD and eventually a hurricane that underwent rapid intensification. These phases are summarized in Figure 28 (timeline).

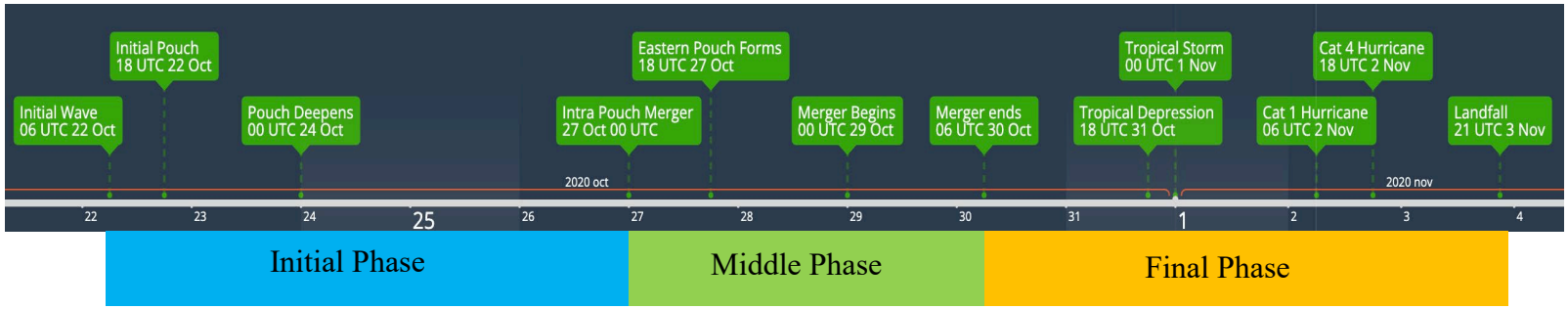

Timeline of the thesis's analysis of the progression of the AEW into Hurricane Eta. Levels tracked for individual analyses are indicated in the text.

Figure 28. Timeline of Eta

The merger was not the only reason this storm continued intensifying. As the two pouches merged, they also entered the eastern Caribbean Sea, an environment with lower vertical wind shear and higher SSTs. These conditions led to a steady intensification of the system until it became a tropical depression at 18 UTC 31 October. After the storm became a TD, a ridge of high pressure developed north of the system, which caused it to move westward for some days (Pasch et al. 2021).

Favorable environmental conditions led the system to rapidly intensify into a tropical storm at 00 UTC 1 November 2020. This was six hours after the system had been declared a tropical depression. When the system became Tropical Storm Eta, it was located 260 n mi southeast of Kingston, Jamaica (Figure 29, top left) (Pasch et al. 2021). Observations show that winds were about 35 kts (Figure 30) and the central pressure was about 1005 mb when the system was declared a TS (Figure 31). At 00 UTC 2 November, a day later, the system's wind speeds had increased to 60 kts (Figure 30) and the central pressure had dropped to about 988 mb (Figure 31). At this time, the system was still a tropical storm on the brink of intensifying to a hurricane.

Tropical Storm Eta continued moving westward, and the NHC declared it a 70 kts category one hurricane by 06 UTC 2 November (Figure 29, top right). Hurricane Eta was located 270 n mi south of Grand Cayman (Pasch et al. 2021), the SST was about 28.8°C (NASA SOTO worldview) and the central pressure had dropped to 982 mb (Figure 31).

After becoming a hurricane, Eta rapidly intensified with a distinct eye by 15 UTC the same day (Pasch et al. 2021). At this time the vorticity was much higher than 6 hours before and also reached deeper into the upper troposphere (Figure 32, right).

By 18 UTC 2 November, pressure had dropped further to 948 mb and winds had increased to up to 115 kts, becoming a category 4 hurricane (Pasch et al. 2021). Eta increased from category 1 to category 4 hurricane in about 12 hours, with over a 45-kts increase in that time period. (Pasch et al. 2021). Hurricane Eta reached peak intensity at 00 UTC 3 November with maximum winds of 130 kts and a central pressure of 929 mb when

it was located 55 n mi east-southeast of Puerto Cabezas, Nicaragua (Pasch et al. 2021). At this time, a mid-level ridge forced Hurricane Eta southwest and slowed its speed.

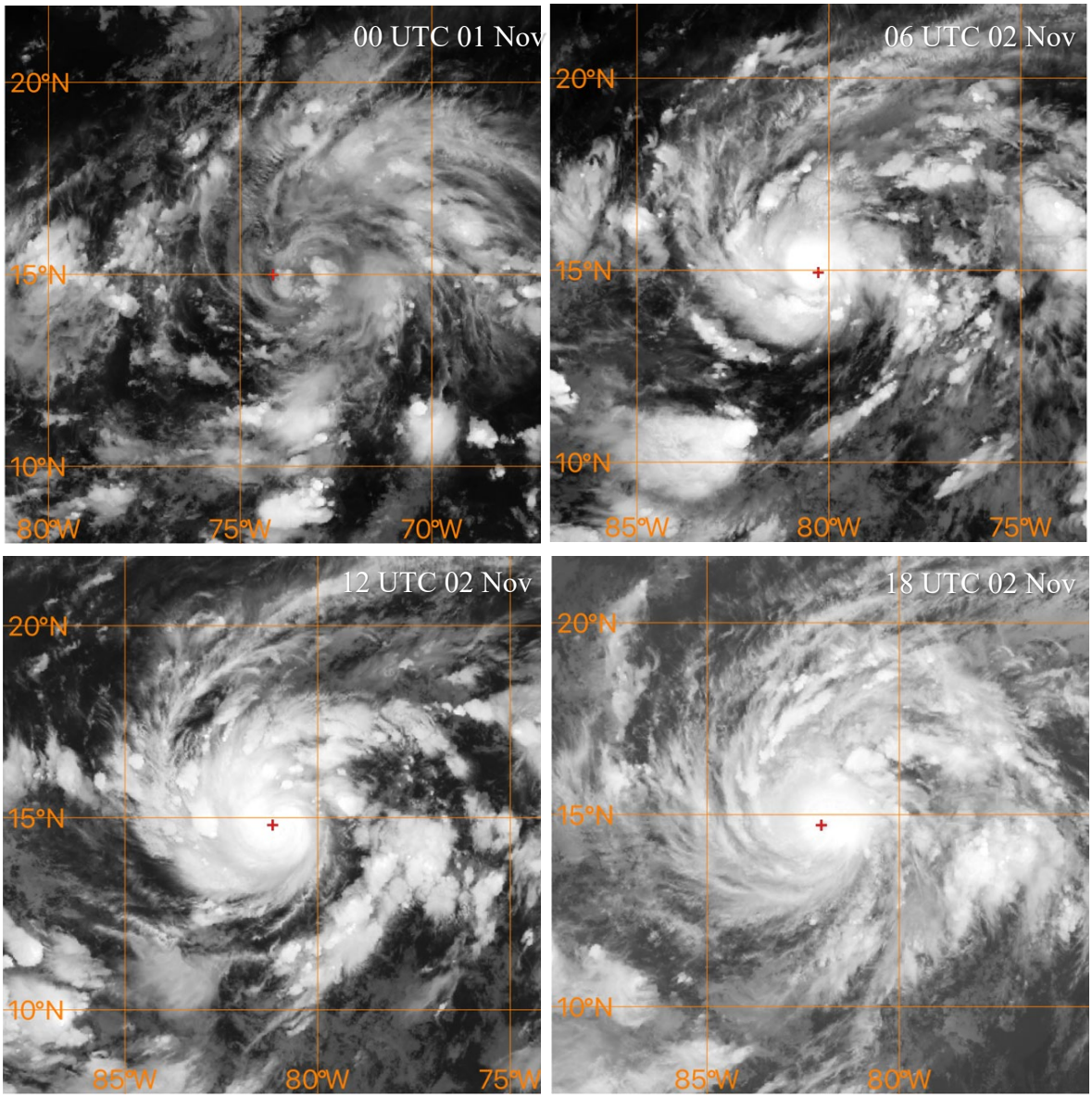

GOES-16 IR imagery at 00 UTC 1 November (top left), 06 UTC 2 November (top right), 12 UTC 2 November (bottom left), and 18 UTC 2 November (bottom right). The red + is the center of OW for the tracked pouch.

Figure 29. Infrared Imagery of the Intensification into Hurricane Eta 1–2 November 2020

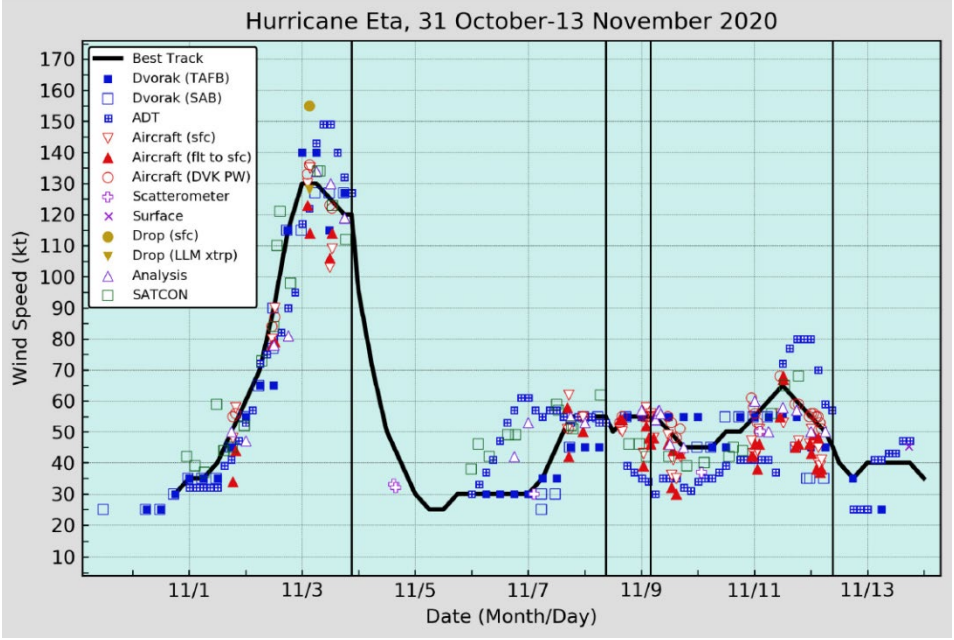

The black line denotes the best track and is an average of the recorded wind speeds from different tools.

Figure 30. Wind Speeds 31 October–13 November 2020. Source: Pasch et al. (2021).

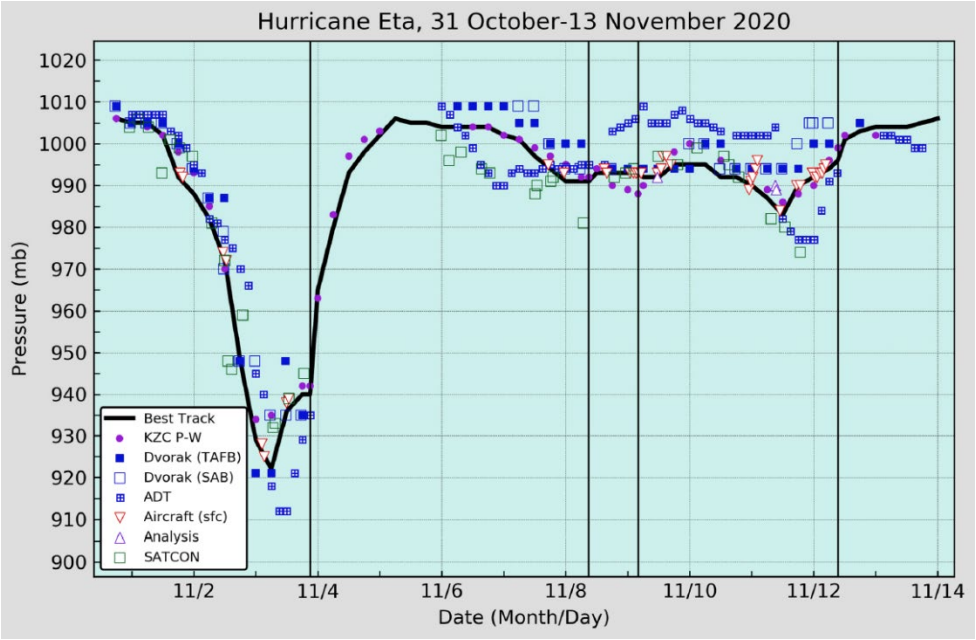

The black line denotes the best track and is an average of the observed values of pressure.

Figure 31. Pressure 31 October–13 November 2020. Source: Pasch et al. (2021).

Six hours later, at 06 UTC 3 November, Hurricane Eta still had max speeds of 130 kt, and the central pressure had dropped to its lowest at 922mb (Pasch et al. 2021). However, at this time there was an eyewall replacement which coincided with a stalling of the system. This decrease in forward speed caused an upwelling of cool coastal waters, weakening the system (Pasch et al. 2021). The combination of these processes decreased the storm's intensity by about 10 kt in 15 hours, after which it proceeded to make landfall as a category 4 hurricane around 15 n mi south-southwest of Puerto Cabezas, Nicaragua at 21 UTC 3 November with 120 kt (Pasch et al. 2021). By 00 UTC 5 November, the storm's winds had quickly decreased after landfall, reaching an average of 30 kt (Figure 30), and the central pressure rapidly increased to 1002 mb (Figure 31).

The NHC defines rapid intensification as "an increase in the maximum sustained winds of a tropical cyclone of at least 30 kt in a 24-h period" (NOAA 2022). Hurricane Eta intensified from 60 kt at 00 UTC 2 November to 130 kt at 00 UTC 3 November, which is a 70 kt increase in 24 hours and a 90 kt increase in 36 hours. Most impressively, it increased from category 1 at 06 UTC 2 November to category 4 at 18 UTC 2 November, which is a 45 kt increase in 12 hours, which is well above the NHC definition for rapid intensification.

This study's third analysis period begins as Eta's precursor pouches merge. Soon after this merger, the vertical mass flux systematically increased with height, as shown by the black line in Figure 32, left. By mass continuity, an increase of the vertical mass flux with height implies there is low-level convergence on the system scale from the beginning of this period. By the classical spin-up mechanism, as discussed in Smith and Montgomery (2023), the system-scale convergence implies that cyclonic relative vorticity is fluxed inwards above the boundary layer. By Stokes' theorem applied to fixed circular loops centered at the pouch center, this inward flux of cyclonic relative vorticity implies that the tangential wind will increase at fixed radii.

The growing mass flux ceases around 00 UTC 2 November, and the vertical structure of the mass flux becomes approximately stationary during the rapid intensification phase starting at 06 UTC 3 November (Figure 32, right panel).

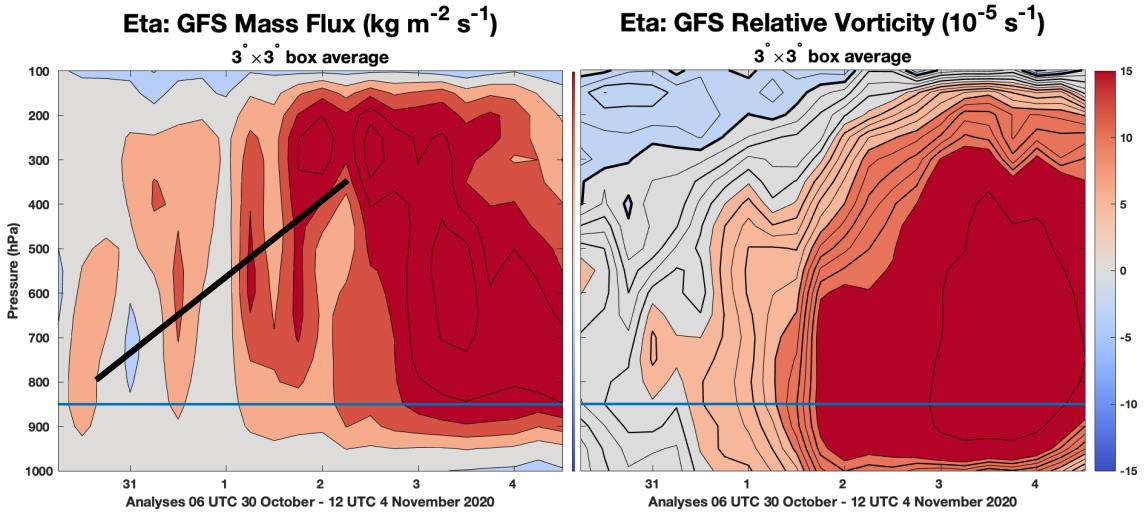

GFS analysis of mass flux (left) and relative vorticity (right) in the 3° x 3° area surrounding Eta's precursor over time. The x-axis represents the time period the precursor was tracked from 06 UTC 30 October to 12 UTC 4 November. The y-axis is height as represented by pressure in mb levels. The intensity of each variable is indicated by the colors with respect to either color bar. The blue horizontal line represents the 850 mb pressure level used to track the system. It is apparent in both plots there is significant mass flux and vorticity after 2 November.

Figure 32. Mass Flux and Relative Vorticity 30 October–4 November 2020

We quantify the areally averaged vertical mass flux (Figure 33, bottom left) and relative vorticity (Figure 33, top left) in both the 3° x 3° and 6° x 6° boxes following the same trend just described in the time height plot. There is an increase in both the vertical mass flux and relative vorticity right before 1 November. The areally averaged OW rapidly increases at the end of 1 November. OW had a distinctive high peak at the end of 2 November when it was declared a category 4 hurricane, although relative vorticity continued increasing after the OW peak (Figure 33, top left).

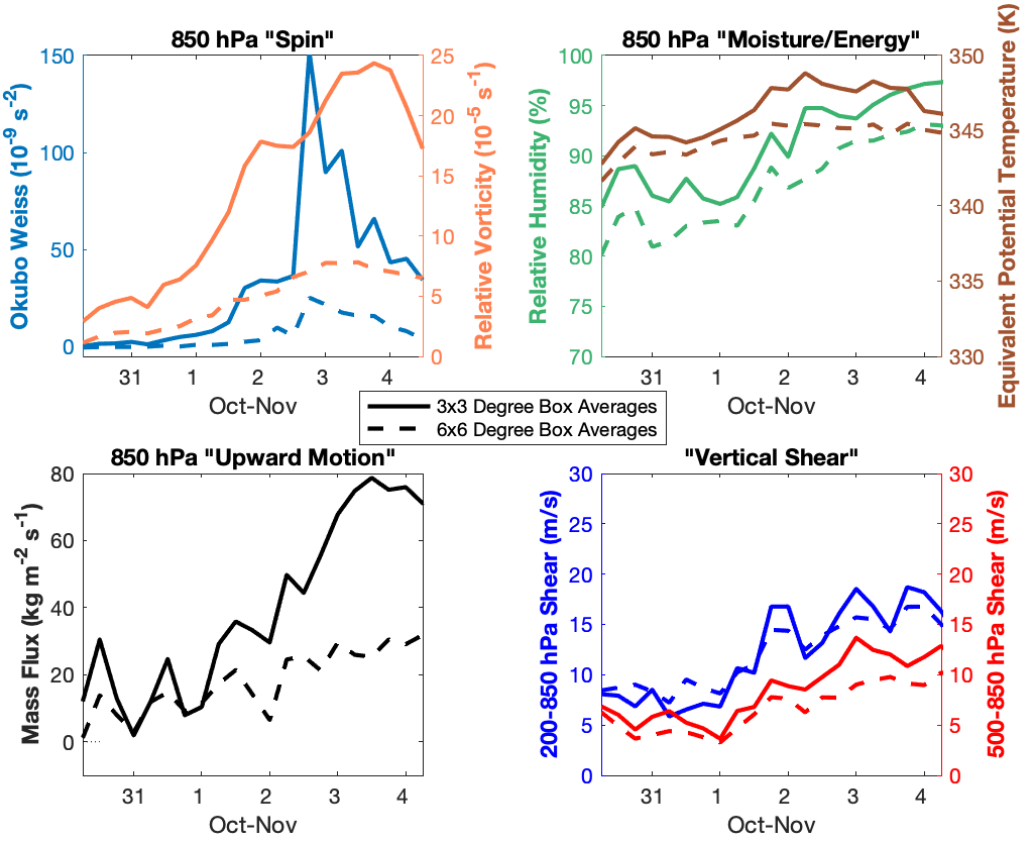

GFS analyses of seven parameters: OW (top left, blue line), relative vorticity (top left, orange line), RH (top right, green line), equivalent potential temperature (top right, brown line), mass flux (bottom left), deep shear (bottom right, blue line), and pouch shear (bottom right, red line) during 18 UTC 30 October to 06 UTC 4 November.

Figure 33. Time Series 30 October–4 November 2020

Both the 200–850 mb deep and 500–850 mb pouch vertical shear are relatively low at the beginning of the time period. The pouch shear ranges from 3 to 5 m s^{-1} until 1 November and then increases progressively as the system intensifies into a hurricane (Figure 33, bottom right). The deep shear ranges from 5 to 10 m s^{-1} until 1 November, when it also increases rapidly. However, this increase in vertical wind shear is an artifact of how the wind shear is calculated. The vertical wind shear calculation averages the shear at multiple points in the boxes. It is not simply the environmental shear, but also includes the shear associated with the developing storm. Because the strengthening vortex is included in this vertical wind shear calculation, we will not analyze the vertical wind shear during the developed phase of hurricanes.

In the time series plot, we also see how the relative humidity in the 3° x 3° box was high since the start of the analysis period, especially after 2 November when it was 95% or higher (Figure 33, top right). The 6° x 6° box was much lower through the period, ranging from 85 to 90%, showing that the highest humidity was located close to the center of the circulation. The equivalent potential temperature was also very high through this period, following a similar trend as relative humidity. The 3° x 3° and 6° x 6° box averages were very close to each other, meaning that the atmosphere had a relatively high amount of moist air moving upwards with high convection (Figure 33, top right).

In the time-height plot of Figure 34, we see indications of instability with decreasing equivalent potential temperature with height in the surface to 600–700 mb level (Figure 34, left). The relative humidity time height plot also shows an increasing RH throughout the period, approaching saturation throughout the column between 2 and 3 December (Figure 34, right).

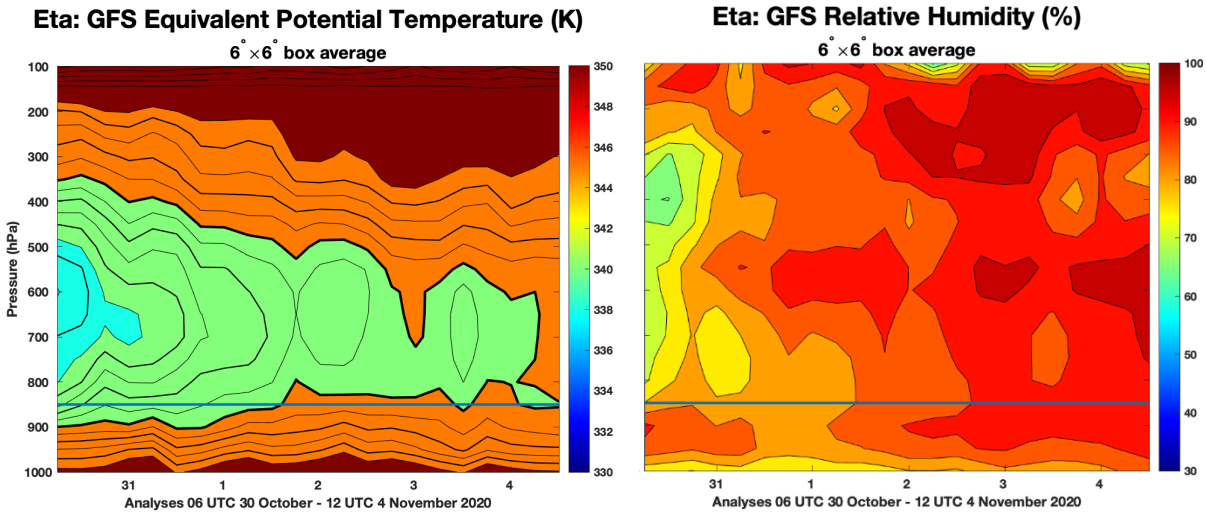

GFS analysis of equivalent potential temperature (left) and relative humidity (right) in the area surrounding Eta's precursor over time. The x-axis represents the time period the precursor was tracked from 06 UTC 30 October to 12 UTC 4 November. The y-axis is height as represented by pressure in mb levels. The intensity of each variable is indicated by the colors with respect to either color bar. The blue horizontal line represents the 850 mb pressure level used to track the system.

Figure 34. Equivalent Potential Temperature 30 October–4 November 2020

THIS PAGE INTENTIONALLY LEFT BLANK

IV. CONCLUSIONS

Hurricane Eta was the most catastrophic hurricane of the 2020 season in the number of casualties and damages. Its rapid intensification took civilians and meteorologists alike by surprise. Between 1950 and 2020, all but one November major hurricane formed and intensified in the Caribbean, exactly what we saw with Hurricane Eta (Klotzbach et al. 2021). Warm SSTs, high relative humidity values, and low vertical wind shear in the eastern Caribbean were amplified in the month of November 2020, which contributed to this system's explosive intensification. Eta would have continued intensifying if not for an eyewall replacement cycle that occurred hours before landfall. Even though this limited its intensity, Hurricane Eta made landfall as a category four hurricane, leaving disaster in its wake.

While the conditions in the Caribbean during November 2020 were conducive to tropical cyclone formation and intensification, the marsupial paradigm explains that the critical ingredient necessary is organized, deep convection within a protective pouch of recirculating air. In this thesis, we analyzed the development of two pouches, which will add to the current knowledge base of the structural formation of pouches and how they relate to TC formation. We found the pouches for Hurricane Eta by selecting the intersection of the wave's trough axis and critical latitude in the wave-pouch comoving frame of reference in GFS analyses. This area has high OW and cyclonic relative vorticity surrounded by closed streamlines of circulation. Although convection was not necessarily directly vertically aligned to the selected pouch center, especially during the early pouch phase, convection was always found in the vicinity of the pouch center. The first pouch was initially identified at the African coast at 700 mb, but it quickly developed to extend through the 700–925 mb layer. However, this pouch gradually weakened and lost its circulation at 700 mb, which led to a decrease in convection associated with the pouch. Once this originally tracked pouch merged with a recently developed second pouch to its east, the resultant pouch had the deeper vertical extent and strength necessary for tropical cyclone genesis.

The analysis in this thesis demonstrated two pathways leading to the development of Hurricane Eta. The first pathway was caused by an AEW which traveled west into the Atlantic. From this wave, a pouch emerged and entered the ITCZ where it continued developing. The second pathway led to the formation of a secondary pouch via local instability within the ITCZ. The marsupial paradigm supports both pathways that led to the genesis of Eta and ultimately, the merger of these two pouches in the Caribbean provided the conditions needed for Eta's precursor to organize into a TD.

The above summary of an initially solitary pouch that eventually merged with another to form a TD oversimplifies the complex structure of an AEW and its depiction by the GFS model. During the passage of Eta's precursor across the Atlantic, we detected local instability from which two notable features emerged. The first was a pair of OW maxima within our pouch which merged to form a larger pouch. The second notable feature was a separate OW maximum that developed east of our pouch, but ultimately could not become a pouch. This failed pouch was produced by a roll-up of cyclonic relative vorticity. A similar subsequent rollup produced the strong eastern pouch that merged with the weaker pouch to the west, which subsequently led to the creation of Hurricane Eta. More research can be done to understand vorticity evolution and how environmental factors can affect it. Maybe one day, we could forecast vorticity rollups and mergers to improve TC predictions.

The marsupial paradigm suggests a bright future for forecasters due to its ability to identify disturbances with a high likelihood of intensifying into tropical cyclones. The group must continue analyzing storms and learning about the different pathways of pouch emergence and development. The automated system should be improved further to become more autonomous and give more accurate products. For example, the automated system identified Eta's precursor as a pouch at 00 UTC 28 October, which was over five days after we identified the closed circulation of the pouch via visual examination of the GFS fields. Although the pouch software still needs further advancement, the automated system could soon be utilized by forecasters to identify disturbances earlier and improve forecasts across the globe.

LIST OF REFERENCES

American Meteorological Society, 2014: "Vorticity." *Glossary of Meteorology*, https://glossary.ametsoc.org/wiki/Vorticity#:~:text=A%20vector%20measure%20of%20local,and%20%E2%88%87%20the%20del%20operator.

Beven, J. L., R. Berg, and A. Hagen, 2019: Hurricane Michael (AL142018). *National Hurricane Center Tropical Cyclone Report.* https://www.nhc.noaa.gov/data/tcr/AL142018_Michael.pdf

Britton, S., 2021: *An exploration of the Marsupial paradigm in developing African easterly waves from 2020: Josephine, Isaias, and Laura.* M.S. thesis, Dept. of Meteorology, Naval Postgraduate School. http://hdl.handle.net/10945/67674.

Carr, L.E., III, R. L. Elsberry, and M.A. Boothe, 1997: *Condensed and Updated Version of the Systematic Approach Meteorological Knowledge Base Western North Pacific.* Tech. Rep. NPS-MR-98-002, Naval Postgraduate School, Monterey, CA 93943-5114, 167 pp.

Dunkerton, TJ., M. T. Montgomery, and Z. Wang, 2009: Tropical Cyclogenesis in a Tropical Wave Critical Layer: Easterly Waves. *Atmos. Chem. Phys.,* 9, 5587–5646

Emanuel, K.A., 1999: Thermodynamic Control of Hurricane Intensity. *Nature*, 401(6754), 665–669, https://doi.org/10.1038/44326.

Gray, W.M. 1977: Tropical Cyclogenesis in the Western North Pacific. *Journal of the Meteorological Society of Japan,* 5,465-482, 10.2151/jmsj1965.55.5_465

Holton, J.R., 2004: *An Introduction to Dynamic Meteorology*. Elsevier.

Klotzbach, P.J., and Coauthors, 2021: A hyperactive end to the Atlantic hurricane season: October-November 2020. *Bull. Amer. Metero. Soc.,* https://doi.org/10.1175/BAMS-D-20-0312.1.

NASA, 2020: Eta 2020–11-03 0640Z. 10 November 2022, https://worldview.earthdata.nasa.gov/

NASA, 2022: SOTO by World view, 7 Dec 2022. https://soto.podaac.earthdatacloud.nasa.gov/

NOAA, 2020: 06Z Surface Pressure Analysis. NHC, Accessed 18 November 2022, https://ftp.nhc.ncep.noaa.gov/tafb/surface_analysis/2020/10/tsfc_2020102206.pdf

NOAA, 2022: Hurricane Costs. Accessed 09 October 2022, https://coast.noaa.gov/states/fast-facts/hurricane-costs.html.

NOAA, 2022: Weather Glossary: V's. Accessed 19 November 2022, https://www.noaa.gov/jetstream/appendix/weather-glossary-v

NOAA, 2022: Glossary of NHC Terms. Accessed 6 December 2022, https://www.nhc.noaa.gov/aboutgloss.shtml#r

Pasch, R.J., B.J. Reinhart, R. Berg, and D. P. Roberts, 2021: *Hurricane Eta*. National Hurricane Center. https://www.nhc.noaa.gov/data/tcr/AL292020_Eta.pdf

Reeves, M. M., 2019: Tyndall AFB Continues Rebuild Effort One Year after Hurricane Michael. United States Air Force, 1, https://www.af.mil/News/Article-Display/Article/1985948/tyndall-afb-continues-rebuild-effort-one-year-after-hurricane-michael/

Rice, D., 2008: Storm Alert: 'Pouches' Protect Embryonic Hurricanes, *USA Today*, 1.

Smith, R. K., Montgomery, M. T., 2023, *Tropical Cyclones: Observations and Basic Processes*. Elsevier Science.

University of Wisconsin—Madison, 2022: Real-Time Product View: Total Precipitable Water. Accessed 07 October 2022, http://tropic.ssec.wisc.edu/real-time/mtpw2/product.php?color_type=tpw_nrl_colors&prod=globa2&timespan=24hrs&anim=html5

Žagar, N., Skok, G., and Tribbia, J., 2011: Climatology of the ITCZ Derived from ERA Interim Reanalyses. *J. Geophys. Res.*, 116, D15103, doi:10.1029/2011JD015695.

INITIAL DISTRIBUTION LIST

1. Defense Technical Information Center
   Fort Belvoir, Virginia

2. Dudley Knox Library
   Naval Postgraduate School
   Monterey, California